NASA Contractor Report 145304

A THEORETICAL INVESTIGATION OF THE AERODYNAMICS OF LOW-ASPECT-RATIO WINGS WITH PARTIAL LEADING-EDGE SEPARATION

(NASA-CR-145304) A THEORETICAL INVESTIGATION OF THE AERODYNAMICS OF LOW-ASPECT-RATIO WINGS WITH PARTIAL LEADING-EDGE SEPARATION (Kansas Univ. Center for Research, Inc.) 85 p HC A05/MF A01 N78-17993 Unclas G3/02 05951

SUDHIR CHANDRA MEHROTRA AND C. EDWARD LAN

THE UNIVERSITY OF KANSAS CENTER FOR RESEARCH, INC.
LAWRENCE, KS 66044

NASA GRANT NSG-1046
JANUARY 1978

National Aeronautics and
Space Administration

Langley Research Center
Hampton, Virginia 23665

Acknowledgments

The initial financial support by the University of Kansas General Research Allocation No. 3839-5038 for this research is gratefully acknowledged.

Table of Contents

List of Symbols

Symbols	Description	Dimension
a	Percentage movement of a free segment based on the total velocity at its control point	Nondimensional
a_i	Fourier coefficients	Nondimensional
a_ℓ	Leading-edge boundary condition term	Nondimensional
$\vec{a}$	$(x_1 - x)\vec{i} + (y_1 - y)\vec{j} + (z_1 - z)\vec{k}$	m (ft)
$\vec{a}'$	$(x_1 - x)\vec{i} + \beta(y_1 - y)\vec{j} + \beta(z_1 - z)\vec{k}$	m (ft)
A_{ij}	Induced downwash coefficient due to wing	Nondimensional
$\bar{A}$	$\lvert\vec{\ell}'\rvert^2$	m^2 (ft^2)
b	Wing span	m (ft)
$\vec{b}$	$(x_2 - x)\vec{i} + (y_2 - y)\vec{j} + (z_2 - z)\vec{k}$	m (ft)
$\vec{b}'$	$(x_2 - x)\vec{i} + \beta(y_2 - y)\vec{j} + \beta(z_2 - z)\vec{k}$	m (ft)
B_{ik}	Induced downwash coefficient due to leading-edge vortex system	m^{-1} (ft^{-1})
$\bar{B}$	$2(\vec{a}' \cdot \vec{\ell}')$	m^2 (ft^2)
c	Local chord	m (ft)
$\bar{C}$	$\lvert\vec{a}'\rvert^2$	m^2 (ft^2)
$\bar{\bar{c}}$	Mean geometric chord	m (ft)
c_m	Sectional pitching moment coefficient	Nondimensional
c_n	Sectional normal force coefficient	Nondimensional
c_t	Sectional leading-edge thrust coefficient	Nondimensional

Symbols	Description	Dimension
C_L	Total lift coefficient	Nondimensional
C_M	Total pitching moment coefficient	Nondimensional
C_N	Total normal force coefficient	Nondimensional
C_P	Pressure coefficient	Nondimensional
C_R	Root chord	m (ft)
C_T	Total leading-edge thrust coefficient	Nondimensional
C_{D_a}	Induced drag coefficient due to normal force coefficient	Nondimensional
C_{D_b}	Induced drag coefficient due to leading-edge thrust coefficient	Nondimensional
C_{D_i}	Total induced drag coefficient	Nondimensional
C_{L_a}	Lift coefficient due to normal force coefficient	Nondimensional
C_{L_b}	Lift coefficient due to leading-edge thrust coefficient	Nondimensional
F	Force	N (lb)
$\vec{G}_1$	$\dfrac{\vec{a} \times \vec{\ell}}{\lvert \vec{a}' \times \vec{\ell}' \rvert^2} \left\{ \dfrac{\vec{b}'}{\lvert \vec{b}' \rvert} - \dfrac{\vec{a}'}{\lvert \vec{a}' \rvert} \right\} \cdot \vec{\ell}'$	m^{-1} (ft^{-1})
$\vec{G}_2$	$\int_{x'}^{\infty} \dfrac{(\vec{R}_i - \vec{R}) \times d\vec{\ell}}{R_\beta^3}$	m^{-1} (ft^{-1})
F	Force per unit dynamic pressure per unit length	m (ft)
$\vec{\ell}$	$(x_2 - x_1)\vec{i} + (y_2 - y_1)\vec{j} + (z_2 - z_1)\vec{k}$	m (ft)
$\vec{\ell}'$	$(x_2 - x_1)\vec{i} + \beta(y_2 - y_1)\vec{j} + \beta(z_2 - z_1)\vec{k}$	m (ft)

Symbols	Description	Dimension
M	Number of spanwise strips plus one	
M_∞	Free stream Mach number	Nondimensional
N	Number of bound elements	
Na	$N(M - 1)$	
Nb	$(M - 1)$	
Nc	NM	
q	Dynamic pressure, $(\rho V_\infty^2/2)$	N/m^2 (lb/ft^2)
$\vec{q}$	Induced velocity vector due to wing	m/sec (ft/sec)
R_β	$\sqrt{(x_2 - x_1)^2 + \beta^2(y_2 - y_1)^2 + \beta^2(z_2 - z_1)^2}$	m (ft)
$\vec{R}$	$x\vec{i} + y\vec{j} + z\vec{k}$	m (ft)
$\vec{R}'$	$x\vec{i} + \beta y\vec{j} + \beta z\vec{k}$	m (ft)
$\vec{R}_\ell$	$\xi\vec{i} + \eta\vec{j} + \zeta\vec{k}$	m (ft)
$\vec{R}'_\ell$	$\xi\vec{i} + \beta\eta\vec{j} + \beta\zeta\vec{k}$	m (ft)
S	Reference wing area	m^2 (ft^2)
u,v,w	Velocity components	m/sec (ft/sec)
V_∞	Freestream velocity	m/sec (ft/sec)
$\vec{V}$	Induced velocity vector due to leading-edge vortex system	m/sec (ft/sec)
w'	Induced normal wash	m/sec (ft/sec)
x,y,z	Wing rectangular coordinate system with x in the streamwise direction and y to the right	m (ft)

Symbols	Description	Dimension
Z_{min}	Minimum vertical distance of a vortex segment from the wing plane	m (ft)

Greek

α	Angle of attack	rad
β	$\sqrt{1 - M_\infty^2}$	Nondimensional
γ	Vortex density referred to freestream velocity	
Γ	Concentrated vortex strength based on free stream velocity	m (ft)
ΔC_p	Differential pressure coefficient, $(C_{p_{lower}} - C_{p_{upper}})$	Nondimensional
θ	Chordwise angular distance	rad
Λ	Sweep angle of leading-edge	rad
ρ	Fluid density	kg/m^3 $(slugs/ft^3)$
φ	Spanwise angular distance	rad
ψ	Sweep angle of leading-edge vortex element	rad
ξ,η,ζ	Integration variables in cartesian system	m (ft)

Subscripts

1	The first endpoint of a vortex element
2	The second endpoint of a vortex element
B	bound element
cp	Control point

Symbols	Description	Dimension
i	Chordwise bound element number	
j	Spanwise strip number	
k	Chordwise bound element number	
ℓ	Leading-edge	
ℓe	Leading-edge vortex element	
L	Left trailing leg	
R	Right trailing leg	
t	Trailing-edge	
T	Chordwise trailing vortices	

1. Introduction

In recent years increasingly complex wing planforms, which are efficient over a large flight envelope, are being used in the aircraft industry. An efficient high-subsonic or supersonic cruise aircraft must be designed to work efficiently even for off-design performance points, such as, landing and take-off. One way of designing such an aircraft is to have fully attached flow at cruise and controlled leading-edge separation at landing- and take-off-conditions (ref. 1). A significant amount of vortex lift can be generated at high angles of attack by leading-edge vortex flow. Henderson (ref. 1) pointed out that at high angles of attack highly swept-back wings having sharp leading-edges have low amount of leading-edge suction (essentially zero) and generate large amount of vortex lift. However, the leading-edge suction increases as the sweep is decreased or leading-edge radii are increased. The structural considerations restrict the leading-edges to be of finite radii. In these cases the lift data lies between potential and potential plus vortex estimates (zero suction). At present, there exists no theoretical method which can predict aerodynamic characteristics of wings having partial leading-edge suction and vortex flow as mentioned above. A theoretical method is presented here to predict aerodynamic characteristics of wings under such conditions.

A theoretical method for cases with non-zero leading-edge suction and partial leading-edge separation should also be applicable to cases with complete leading-edge separation. Due to lack of data with partial leading-edge separation, the present method has been extensively compared with other theoretical methods and available data only for cases with complete leading-edge separation. Thus, a survey of literature on completely separated leading-edge vortex flow seems pertinent.

Legendre (ref. 2) was the first one who attempted to solve the leading-edge separation problem. He assumed that rolled up vortex sheets over the wing can be replaced by a pair of concentrated vortices (fig. 1). In this model the flow tangency boundary condition over the wing was satisfied along with the leading-edge Kutta condition. The flow was assumed to be conical so that conformal mapping could be used. Upon the instigation by Adams (ref. 3), Legendre (ref. 4) revised his model. He reported that in his first model he had assumed a cut joining the two vortices. In another form of his model, Legendre included a cut between the vortices and their respective leading-edges to account for the feeding sheets. Adams pointed out that in the first model of Legendre the lift was multivalued because the region was no longer simply connected and in the second one the pressure difference was allowed across the sheet. Based on the suggestions of Edwards (ref. 5), Brown and Michael (ref. 6) modified Legendre's slender body model by using feeding cuts, which connected the line vortices to the wing leading-edges (fig. 2). This vortex system of concentrated line vortex and feeding cuts was required to satisfy the force free condition. The leading-edge Kutta condition and flow tangency boundary condition on the wing were also satisfied. Mangler and Smith (ref. 7) proposed a somewhat more realistic model than that of Brown and Michael, but still used slender body theory in their investigation. They used a continuous model of the separated vortex sheet along with a concentrated core (fig. 3). The shape and strength of the vortex sheet and the concentrated line vortex were determined by satisfying the flow tangency condition on the wing and the pressure continuity condition across the separated vortex sheet. Later, Smith (ref. 8) used segmented feeding vortex sheet with considerable improvement in numerical procedure (fig. 4), largely due to advent of greater computing power. The above model was modified further for thick wings (Smith, ref. 9). The main shortcoming of all these models described so far is the assumption of conical flow.

Gersten (ref. 10) extended Bollay's vortex model (ref. 11), which was for rectangular wings with wing tip separation, to arbitrarily shaped wings of small aspect ratio with leading-edge separation (fig. 5). In this model the vortices came off wing edges at an angle $\alpha/2$ to the wing plane. The wing was replaced by infinitesimal lifting elements and the strength of vortices was assumed to vary along the span. At this point the flow tangency condition on the wing was satisfied to find the wing characteristics. Garner and Lehrian (ref. 12) followed Gersten's approach by using Multhopp's lifting surface theory (ref. 13) to represent the wing. Both of these models are very crude and give only total characteristics of the wing; i.e., pressure distributions are not calculated.

Sacks, et al (ref. 14) assumed aerodynamic characteristics (lift and pitching moment) to be composed of two components - the linear and non-linear components. The linear component was calculated by using the integral method of Lawrence (ref. 15), while the non-linear component was calculated by assuming that vortex pairs were shed just outside the wing leading-edge with shedding rate determined by either an empirical method or slender wing theory. The location of each vortex pair was determined by satisfying the force free condition at the vortices.

Nangia and Hancock (ref. 16) extended Brown and Michael's model (ref. 6) to non-slender wings. In their model the wing planform was represented by bound- and trailing-vorticity distributions. The wake behind the trailing-edge was free to move outboard and the leading-edge separation was represented by two isolated vortices, which were connected to the leading-edge by cuts (as in Brown and Michael). The Kutta condition was satisfied along the leading- and trailing-edges and the flow tangency condition was satisfied on the wing surface. Zero force condition was satisfied on the isolated vortices and the cuts at selected collocation points. Although this method was not restricted to slender wings, the leading-edge flow model was crude.

Polhamus (ref. 17 and 18) used leading-edge suction analogy to predict lift coefficients for various simple planforms, such as, arrow-, diamond- and delta-wings. It was assumed that when the complete flow reattachment occurs inboard of the leading-edge vortices, the total lift equals the sum of the potential and vortex lift. These components of lift were calculated by using a modified form of Multhopp's lifting surface theory (ref. 19). The vortex lift was assumed to be equal in magnitude to the potential flow leading-edge suction force lost due to separation. In its original form this method did not calculate the local distribution of lift and so the pitching moments were not predicted. Snyder and Lamar (ref. 20) used this method to predict the longitudinal load distribution and pitching moment for delta wings.

Mook and Maddox (ref. 21) modeled the leading-edge vortex system by finite vortex elements coming off the leading-edge (fig. 6). This network of vortex elements was superimposed on the vortex-lattice used by Giesing, et al (ref. 22). The solution is obtained in an iterative manner by satisfying the flow tangency boundary condition on the wing surface, approximately satisfying leading- and trailing-edge Kutta conditions, and satisfying force free conditions on the vortex elements over the wing surface. The force free condition was not satisfied on the wake behind the trailing-edge. Kandil, et al (ref. 23) modeled the flow in a manner similar to that of Mook and Maddox (ref. 21) and extended it to wing-tip seperation also. Kandil, et al followed Belotserkovskii (ref. 24) for the representation of the wing surface. In this model the bound elements of the vortex-lattice were unswept, and the wake behind the trailing-edge and the vortex elements coming from wing-tip were force free. Apparently, this method has been restricted to an angle of attack of 20 degrees (ref. 25). Kandil, et al (ref. 26) extended their model to calculate the location and strength of a concentrated core, which they also used for convergence criteria. Rehbach (ref. 27) also followed Belotserkovskii to model wing-tip separation and the approach was similar to that of Kandil, et al (ref. 23). However, he solved the leading-edge separation problem differently (ref. 28). The process was started by finding a converged solution for a rectangular wing (fig. 7). The leading-edge span of the rectangular wing was decreased by a small amount, while the trailing-edge span was kept constant. A new converged solution for this wing was obtained. This process was repeated until the planform reduced to a delta wing. The deficiency of these methods is that the leading-edge Kutta condition is only approximately satisfied. The iteration process of Rehbach could also be quite time consuming.

Nathman (ref. 29) presented two models of leading-edge separation; the fixed wake model and the free wake model (fig. 8). In both models the wing was represented by panels with constant strength doublet distribution, being equivalent to closed vortex filaments on the boundary of the panels. In the fixed wake model the separated sheet was modeled by placing a series of planar boxes along the leading-edge which extended to the vortex core predicted analytically by Brown and Michael (ref. 6). The doublet strengths were obtained by satisfying flow tangency boundary conditions only. In the free wake model the separated vortex sheet was represented by discrete vortices attached to the leading-edge. These vortices were aligned along the local velocity vector to be force free. The wake behind the trailing-edge was force free only to a certain extent. The fixed wake model is too crude, whereas no definite convergence criteria has been established for the free wake model.

The most sophisticated and realistic model of all leading-edge separation models has been due to Brune, et al (ref. 30). In this model the wing and the separated vortex sheet were represented by piecewise continuous doublet distributions. The separated vortex sheet was connected to a concentrated core by a continuous fed sheet (fig. 9). The solution was obtained in an iterative manner by satisfying the Kutta condition along all edges, flow tangency boundary condition on the wing, and the force free condition on the separated vortex sheet and wake behind the trailing-edge. This model has also been extended to thick and cambered wings. The drawbacks of this model are that it cannot predict lift correctly at small angles of attack for moderate to low aspect ratio wings, takes too much computer time to get a converged solution and needs large computer memory space.

All methods mentioned above calculate only the wing characteristics for complete loss of leading-edge suction. A method is developed here for partial leading-edge flow separation with non-zero leading-edge suction. The wing boundary condition is formulated by the Quasi Vortex Lattice method (QVLM) of Lan (ref. 31). The advantage of this method is that the leading-edge boundary condition can be exactly satisfied. The leading-edge separated vortices are represented by discrete free vortex elements which are aligned with the local velocity vector at their mid-points to satisfy the force free condition. The wake behind the trailing-edge is also force free. The flow tangency boundary condition is satisfied on the wing, including the leading- and trailing-edges. Due to the non-linear nature of the problem, the problem is solved in an iterative manner. Due to non-availability of any data with partial leading-edge separation, the method will be compared only with other methods (ref. 32 and 33) and experimental data (ref. 34 thru 40) for complete leading-edge separation. The basic assumption in the present theory is that the Prandtl-Glauert equation is applicable. The thickness and fuselage effects are ignored.

Chapter 2 presents the theoretical method. In Chapter 3, numerical results are presented and discussed. Conclusions and recommendations are made in Chapter 4.

2. Theoretical Method

2.1 Problem Definition

In steady symmetric flight at a high angle of attack, the flow over a thin low aspect ratio highly sweptback wing separates along the leading-edge and the tips. In the following, only delta wings will be considered. The wing can be represented by a bound vortex sheet, across which exists a pressure difference, and the separated flow along leading-edges by force free vortex sheets, across which there is no pressure difference. In the present method, the Quasi-Vortex-Lattice method (ref. 31) is used to simplify the induced velocity expressions due to the bound vortex sheet and discrete force free vortex elements for separated vortex sheets.

The following boundary conditions are imposed on the flow model:

a. The flow must be tangential to the wing camber surface.

b. The leading-edge boundary condition and trailing-edge Kutta condition are to be satisfied.

c. The vortex elements over the wing and wake behind the trailing-edge are force free.

This is a non-linear problem because the strengths of the wing bound vortices and free vortices, and the locations of the free vortex elements are unknown. Thus, the problem is solved by an iterative method.

2.2 Model Geometry

The origin of the rectangular coordinate system is at the wing apex. The wing lies in the x-y plane and the x-axis is taken along the wing center-line. The wing span is given by b and the surface area by S.

2.2.1 Wing Geometry

The location of bound- and trailing-vortex elements for a typical case are shown in figure 10, a detailed description of which is given in section 2.3. The x-location of bound elements is given by the cosine law and is illustrated in figure 10.

$$x_i = x_\ell + \frac{c}{2}\left(1 - \mathrm{Cos}\left(\frac{2i - 1}{2N}\pi\right)\right), \qquad (2.1)$$

$$i = 1,2,---N$$

where x_ℓ is the leading-edge x-coordinate, c is the chord and N is the number of bound elements in a chordwise direction. The spanwise location of trailing elements is given by,

$$y_j = \frac{b}{4}\left(1 - \mathrm{Cos}\left(\frac{2j - 1}{2M}\pi\right)\right), \qquad (2.2)$$

$$j = 1,2,---M$$

where b is the span and M is the number of legs of trailing vorticity, which is one higher than the number of spanwise strips of bound elements. The locations of control points are given by,

$$x_{cp_k} = x_{\ell_j} + \frac{c_j}{2} (1 - \mathrm{Cos}(\frac{\pi k}{N})) \; , \tag{2.3}$$

$$k = 0,1,2,\text{---}N$$

$$y_{cp_j} = \frac{b}{4} (1 - \mathrm{Cos}(\frac{\pi j}{M})) \; , \tag{2.4}$$

$$j = 1,2,\text{---}(M - 1)$$

where x_{ℓ_j} and c_j are the leading-edge x-coordinate and chord at y_{cp_j} respectively.

2.2.2 Leading-Edge Vortex System Geometry

The leading-edge vortex system is superimposed on the regular quasi-vortex-lattice grid. A typical vortex element is shown by points A through J in figure 11. These points are connected by a series of short straight segments. The initial location of these segments is shown by dashed lines and final location by solid lines. These segments have the following characteristics:

a. Points A through E lie along a wing trailing vortex element. Initially point A is one root chord away from the trailing-edge in the downstream direction and the line segments between A and D are parallel to the axis of symmetry. The line segments between points A and B are of equal length. In the final converged position these segments are aligned in the direction of the local velocity vector. The segments B-C and C-D are 0.1 C_R long. B-C is allowed to move only in the vertical direction whereas C-D is fixed in the wing plane because flow is tangential to the trailing-edge. Segment D-E is also fixed in the wing plane.

b. Points E, F, G and H also lie in the wing plane. The location of segment E-F is ahead of the wing first bound element and is given by,

$$x_E = x_{\ell_E} + \frac{c_E}{2} \left(1 - \mathrm{Cos}\left(\frac{\pi}{2(N + 1)}\right)\right) \tag{2.5a}$$

$$x_F = x_{\ell_F} + \frac{c_F}{2} \left(1 - \mathrm{Cos}\left(\frac{\pi}{2(N + 1)}\right)\right) \tag{2.5b}$$

where the subscripts E and F refer to the points under consideration. The above two equations are similar to equation (2.1). It is to be noted that segment E-F is located at the first bound element for a grid of (N + 1) bound elements in a chordwise direction. The segments F-G and G-H are of the same length and point G lies on the leading-edge. The segment G-H is fixed in the wing plane due to the leading-edge boundary condition.

c. The initial location of point I is given by,

$$x_I = x_F \tag{2.6a}$$

$$y_I = y_F \tag{2.6b}$$

$$z_I = 0.1\ C_R \tan(22.5 - 0.5\alpha) \quad \text{for} \quad \alpha \leq 15^\circ \tag{2.6c}$$

or $$z_I = 0.1\ C_R \tan\alpha \quad \text{for} \quad \alpha \geq 15^\circ \tag{2.6d}$$

where C_R is the root chord and α is the angle of attack. Initially point J is one root chord away from the trailing-edge. The segments between point I and J are of equal length and lie in a plane parallel to x-z plane. These segments are approximately at a height of 0.1 C_R above the wing plane (see Chapter 2.6). In the final converged position all the segments between points H and J are aligned in the direction of the local velocity vector.

d. The semi-infinite segments from points A to infinity and J to infinity are straight and are parallel to the undisturbed free-stream direction.

2.3 Induced Velocity Due to Wing

In the quasi-vortex-lattice method (ref. 31), for the purpose of satisfying wing boundary (tangency) condition, the continuous vortex distribution over the wing is replaced by a quasi-continuous one, being continuous chordwise but stepwise constant in the spanwise direction. Thus, the wing surface can be divided into a number of vortex strips with the associated trailing vortices (fig. 10). In any strip, consider a vortex element γdx with an arbitrary direction $\vec{\ell}$ (fig. 12). The induced velocity due to all bound elements in ith strip is given by (see Appendix A),

$$\vec{q}_{i_1}(\vec{R}) = \frac{\beta^2}{4\pi} \int_{x_\ell}^{x_t} \gamma(x') \left(\frac{\vec{a} \times \vec{\ell}}{|\vec{a}' \times \vec{\ell}'|^2} \left\{ \frac{\vec{b}'}{|\vec{b}'|} - \frac{\vec{a}'}{|\vec{a}'|} \right\} \cdot \vec{\ell}' \right) dx' \qquad (2.7)$$

and due to the associated trailing vortices by (ref. 31),

$$\vec{q}_{i_2}(\vec{R}) = \frac{\beta^2}{4\pi} \int_{x_\ell}^{x_t} \gamma(x') \left(\int_{x'}^{\infty} \frac{(\vec{R}_i - \vec{R}) \times d\vec{\ell}}{R_\beta^3} \right) dx' \qquad (2.8)$$

The transformation, $x' = x_\ell + \frac{c(y)}{2}(1 - \text{Cos}\,\theta)$, reduces equations (2.7) and (2.8) to,

$$\vec{q}_{i_1}(\vec{R}) = \frac{\beta^2 c(y)}{8\pi} \int_o^\pi \vec{G}_1(\theta)\, \gamma(\theta)\, \text{Sin}\,\theta\, d\theta \qquad (2.9)$$

and

$$\vec{q}_{i_2}(\vec{R}) = \frac{\beta^2 c(y)}{8\pi} \int_o^\pi \vec{G}_2(\theta)\, \gamma(\theta)\, \text{Sin}\,\theta\, d\theta \qquad (2.10)$$

where,

$$\vec{G}_1(\theta) = \frac{\vec{a} \times \vec{\ell}}{|\vec{a}' \times \vec{\ell}'|^2} \left\{\frac{\vec{b}'}{|\vec{b}'|} - \frac{\vec{a}'}{|\vec{a}'|}\right\} \cdot \vec{\ell}'$$

$$\vec{G}_2(\theta) = \int_{x'}^{\infty} \frac{(\vec{R}_i - \vec{R}) \times d\vec{\ell}}{R_\beta^3}$$

and $c(y) = x_t - x_\ell$. $\vec{a}$, $\vec{b}$, etc. are defined in the List of Symbols. The total induced velocity due to the ith strip of vortex distribution is given by,

$$\vec{q}_i(\vec{R}) = \frac{\beta^2 c(y)}{8\pi} \int_o^\pi \vec{G}_1(\theta)\, \gamma(\theta) \text{ Sin } \theta \, d\theta$$

$$+ \frac{\beta^2 c(y)}{8\pi} \int_o^\pi \vec{G}_2'(\theta)\, \gamma(\theta) \text{ Sin } \theta \, d\theta$$

$$- \frac{\beta^2 c(y)}{8\pi} \int_o^\pi \vec{G}_2''(\theta)\, \gamma(\theta) \text{ Sin } \theta \, d\theta \qquad (2.11)$$

where the first term is due to bound elements, second due to left leg of trailing elements and third due to the right leg of trailing elements. The above integrals are reduced to finite sums through the midpoint trapezoidal rule (see ref. 31):

$$\vec{q}_i(\vec{R}) = \frac{\beta^2 c(y)}{8N} \sum_{k=1}^{N} (\vec{G}_{1_k} + \vec{G}_{2_k}' - \vec{G}_{2_k}'')\gamma_k \text{ Sin } \theta_k \qquad (2.12)$$

where $\theta_k = \frac{(2k - 1)}{2N} \pi$ and locations of bound elements are given by,

$$x_{1_k} = x_{\ell_1} + c_1\xi_k \tag{2.13a}$$

$$x_{2_k} = x_{\ell_2} + c_2\xi_k \tag{2.13b}$$

$$\xi_k = \frac{1}{2}\,[1 - \mathrm{Cos}(\frac{2k-1}{2N}\,\pi)],\ k = 1,2,\text{---},N \tag{2.13c}$$

x_{ℓ_1} = the leading edge x-coordinate at y_1 (left leg)

x_{ℓ_2} = the leading edge x-coordinate at y_2 (right leg)

c_1 = chord length at y_1

c_2 = chord length at y_2

The control points in the chordwise direction are chosen such that,

$$x_i = x_\ell + \frac{c}{2}\,(1 - \mathrm{Cos}\,\frac{i\pi}{N}),\ i = 1,2,\text{---}N \tag{2.14}$$

where x_ℓ is the leading edge x-coordinate on the chord c through the control point. The spanwise location of trailing vortices is given by,

$$y_j = \frac{b}{4}\,(1 - \mathrm{Cos}(\frac{2j-1}{2M}\,\pi)),\ j = 1,2,\text{---}M \tag{2.15}$$

and control points by,

$$y_i = \frac{b}{4}\,(1 - \mathrm{Cos}(\frac{i\pi}{M})),\ i = 1,2,\text{---}(M-1) \tag{2.16}$$

where b is the span and M is the total number of trailing vortices which is one more than spanwise strips. The geometry associated with equations (2.13) - (2.16) is based on the semi-circle method and is illustrated in figure 10.

Thus, induced velocity due to all vortex strips of the wing can be written as,

$$\vec{q}(\vec{R}) = \sum_{i=1}^{M-1} \vec{q}_i(\vec{R}) \tag{2.17}$$

2.4 Induced Velocity Due to Leading-Edge Vortex System

The leading-edge vortex system, as described in Chapter 2.2.2, consists of "M-1" elements. Each element may have different number of small vortex segments. Assume that ith set has L small segments. The induced velocity at a point (x,y,z) due to jth segment of ith element is given by (Appendix A),

$$\vec{V}_{i_j}(\vec{R}) = \frac{\beta^2 \Gamma_i}{4\pi} \frac{\vec{a} \times \vec{\ell}}{|\vec{a}' \times \vec{\ell}'|^2} \left\{\frac{\vec{b}'}{|\vec{b}'|} - \frac{\vec{a}'}{|\vec{a}'|}\right\} \cdot \vec{\ell}' \tag{2.18}$$

where

$$\vec{R} = x\vec{i} + y\vec{j} + z\vec{k}$$

$$\vec{a} = (x_j - x)\vec{i} + (y_j - y)\vec{j} + (z_j - z)\vec{k}$$

$$\vec{b} = (x_{j+1} - x)\vec{i} + (y_{j+1} - y)\vec{j} + (z_{j+1} - z)\vec{k}$$

$$\vec{\ell} = (x_{j+1} - x_j)\vec{i} + (y_{j+1} - y_j)\vec{j} + (z_{j+1} - z_j)\vec{k}$$

$$\vec{a}' = (x_j - x)\vec{i} + \beta(y_j - y)\vec{j} + \beta(z_j - z)\vec{k}$$

$$\vec{b}' = (x_{j+1} - x)\vec{i} + \beta(y_{j+1} - y)\vec{j} + \beta(z_{j+1} - z)\vec{k}$$

$$\vec{\ell}' = (x_{j+1} - x_j)\vec{i} + \beta(y_{j+1} - y_j)\vec{j} + \beta(z_{j+1} - z_j)\vec{k}$$

Γ_i = Vortex strength of ith set of segments

The subscripts j and $j+1$ correspond to the end points of jth segment.

Now the induced velocity due to ith element can be written as,

$$\vec{V}_i(\vec{R}) = \sum_{j=1}^{L} \vec{V}_{i_j}(\vec{R}) \tag{2.19}$$

Therefore, the induced velocity due to all elements is,

$$\vec{V}(\vec{R}) = \sum_{i=1}^{M-1} \vec{V}_i(\vec{R}) \tag{2.20}$$

2.5 Boundary Conditions

The two basic boundary conditions to be satisfied in the model are,

a. The flow must be tangential to the wing camber surface.

b. The vortex elements above the wing and in the wake behind the trailing-edge must be force free.

2.5.1 Formulation Of Wing Boundary Condition

The bound elements and the corresponding control points of the wing surface are numbered from the leading-edge to the trailing-edge and from the root to the tip. Thus, there are $Na = N(M - 1)$ bound elements and corresponding control points (see Chapter 2.2.1). Similarly, the vortex elements and the corresponding control points in the leading-edge vortex system are numbered from the root to the tip. There are $Nb = (M - 1)$ leading-edge vortex elements being equal to the number of wing vortex strips. Thus, there must be $Nc = Na + Nb$ control points on the wing surface. The flow tangency condition can be written as,

$$\underset{NcxNa}{[A_{ij}]}\ \underset{Nax1}{\{\gamma_j\}} + \underset{NcxNb}{[B_{ik}]}\ \underset{Nbx1}{\{\Gamma_k\}} = \underset{Nc \times 1}{\left\{ \begin{array}{c} \left(\frac{dz}{dx}\right)_i - \sin\alpha \\ \hline a_{\ell_k} + \left(\frac{dz}{dx}\right)_k - \sin\alpha \end{array} \right\}} \begin{array}{c} \updownarrow Na \\ \updownarrow Nb \end{array} \qquad (2.21)$$

where A_{ij} is the induced downwash at ith control point of wing due to a unit horseshoe vortex density at j; B_{ik} the induced downwash at ith control point due to kth leading-edge vortex element of unit strength; γ_j the vortex density of the jth bound element; Γ_k the strength of kth leading-edge vortex element, $\left(\frac{dz}{dx}\right)_i$ the camber slope at the ith control point and α the angle of attack. According to equations (52) and (53) of ref. 31, the leading-edge thrust coefficient is related to the normalwash on the leading edge by the following equation:

$$a_{\ell_k} = \text{induced normalwash} - \left(\frac{dz}{dx}\right)_k + \sin\alpha \tag{2.22}$$

which leads to the last expression on the right hand side of equation (2.21). In the above expression, a_ℓ is defined as:

$$a_{\ell_k} = N\sqrt{\tan^2\Lambda + \beta^2}\left(\frac{2\, c_{t_k} \cos\Lambda}{\pi\sqrt{1 - M_\infty^2 \cos^2\Lambda}}\right)^{1/2} \tag{2.23}$$

N = Number of chordwise vortex elements

Λ = Leading-edge sweep angle

M_∞ = Free stream Mach number

$\beta = \sqrt{1 - M_\infty^2}$

c_{t_k} = Sectional leading-edge thrust coefficient of the kth strip

For complete leading-edge separation cases the sectional leading-edge suction is zero and so is a_{ℓ_k}.

2.5.2 Formulation Of Force Free Condition Of Free Elements

The vortex segments above the wing surface and the wake are to be aligned in the direction of local velocity vector calculated at their mid-points. Consider ith segment of a vortex element. The coordinates of its end points are given by (x_i, y_i, z_i) and $(x_{i+1}, y_{i+1}, z_{i+1})$. Assume that the velocity at the mid-point of this segment at a given iterative step is given by,

$$\cdot \quad (u\vec{i} + v\vec{j} + w\vec{k})$$

Then, the new location of the (i + 1)th end point will be,

$$x_{i+1_N} = x_i + \frac{u}{U} \Delta s \tag{2.24a}$$

$$y_{i+1_N} = y_i + \frac{v}{U} \Delta s \tag{2.24b}$$

$$z_{i+1_N} = z_i + \frac{w}{U} \Delta s \tag{2.24c}$$

where

$$U = \sqrt{u^2 + v^2 + w^2}$$

and

$$\Delta s = \sqrt{(x_{i+1} - x_i)^2 + (y_{i+1} - y_i)^2 + (z_{i+1} - z_i)^2}$$

Before equations (2.21) are used, the following points should be considered:

a. The length of each segment is to be preserved.

b. The free vortex segments above the wing should not come too close to the wing surface to avoid numerical difficulty in the present inviscid theory.

c. The adjustment of the location of each segment to satisfy the force free condition should be such that it does not result in numerical fluctuations (see Chapter 2.6).

Based on the above consideration, equations (2.24) will be modified as follows.

Consider the same ith segment. If this segment moves a-percent only according to the velocity computed at its mid-point, then equations (2.24) can be modified to be,

$$\Delta y_N = \frac{av}{U} \Delta s + (1 - a)(y_{i+1} - y_i) \tag{2.25a}$$

$$\Delta z_N = \frac{aw}{U} \Delta s + (1 - a)(z_{i+1} - z_i) \tag{2.25b}$$

$$\Delta x_N = \sqrt{\Delta s^2 - \Delta y_N^2 - \Delta z_N^2} \tag{2.25c}$$

It follows that,

$$x_{i+1_N} = x_i + \Delta x_N \tag{2.26a}$$

$$y_{i+1_N} = y_i + \Delta y_N \tag{2.26b}$$

$$z_{i+1_N} = z_i + \Delta z_N \tag{2.26c}$$

Let Z_{min} be the minimum vertical distance any vortex segment is allowed to come close to the wing surface. If z_{i+1_N} is less than Z_{min}, it is then set equal to Z_{min} and Δz_N is recalculated by using,

$$\Delta z_N = Z_{min} - z_i \tag{2.27}$$

This value of Δz_N is used to calculate x_{i+1_N}.

2.6 Solution Procedure

The basic unknowns of the problem are the bound vortex density on the wing, and the strengths and the locations of the elements of the leading-edge vortex system and the wake. The problem is non-linear because the locations of the leading-edge vortex system and the wake are unknown a priori. Therefore, the problem will be solved by the iterative process described below;

a. Prescribe the vortex lattice for the wing surface, and the initial locations of the free elements over the wing and in the wake.

b. By satisfying the wing boundary condition, i.e. equation (2.21), obtain the bound vortex density of the wing and the strengths of free elements.

c. Calculate all the aerodynamic characteristics.

d. Calculate the forces acting on the free elements over the wing surface.

e. Adjust the free elements of the leading-edge vortex system and the wake in the local velocity vector direction, as described in Chapter 2.5.2.

f. Repeat steps b through e until a converged solution is obtained.

The initial locations of the free vortex elements are assumed by letting them leave the leading-edge in the undisturbed free-stream direction up-to a height of about ten percent of the root chord beyond which the elements are parallel to the wing plane. Initially, all the elements of the wake lie in the plane of the wing. In the iteration process, the force free condition is satisfied on the free elements from the root to the tip in the down-stream direction. A similar approach has been used by Butler and Hancock (ref. 41) with success for the wake problem. The elements over the wing are adjusted before the elements of the wake. In the first iteration the segments over the wing are moved 100 percent according to the velocity computed at their mid-points. This movement is gradually reduced in steps of 90, 80 and 75 percent in the next three iterations, after which it remains at 75 percent (see equations (2.25) and (2.26)). The segments in the wake are moved only 50 percent in each iteration. Thus, exact force free condition is not enforced because whenever the free elements come close to each other they induce unreasonably large velocities because viscous effects are not included in the present theory. These large velocities increase the forces on the elements and induce fluctuations in their locations.

The solution is assumed to have converged if in two consecutive iterations the difference between the total strengths of leading-edge free vortex elements is less than one percent and the absolute force acting on the free elements is in the neighborhood of a minimum. Thus, an exact force free condition is not enforced as discussed in the previous paragraph.

2.7 Aerodynamic Characteristics

The expressions for the evaluation of the pressure distribution are derived in Appendix B. They are obtained by applying the Kutta-Joukowski theorem to the vortex system on the wing.

The sectional normal force coefficient of jth strip is given by chordwise integration of the differential pressure coefficient:

$$c_{n_j} = \frac{1}{c_j} \int_{x_{\ell_j}}^{x_{t_j}} \Delta C_p \, dx \tag{2.28}$$

where x_{ℓ_j} and x_{t_j} are the leading and trailing edge x-coordinates of the chord passing through the control points of the jth strip and c_j is the chord length. The transformation,

$$x = x_{\ell_j} + \frac{c_j}{2} (1 - \mathrm{Cos}\ \theta) \tag{2.29}$$

reduces equation (2.28) to:

$$\begin{aligned} C_{n_j} &= \frac{1}{2} \int_o^{\pi} \Delta C_p \ \mathrm{Sin}\ \theta \ d\theta \\ &\cong \frac{\pi}{2(N+1)} \sum_{k=1}^{N+1} \Delta C_{p_k} \ \mathrm{Sin}\ \theta_k \end{aligned} \tag{2.30}$$

and

$$\theta_k = \frac{(2k - 1)}{2(N + 1)} \pi, \ k = 1,2,---(N+1)$$

where the midpoint trapezoidal rule has been used to reduce the integral to a finite sum. Similarly, the sectional pitching moment coefficient for the jth strip about the y-axis is given by,

$$c_{m_j} = -\frac{1}{c_j\bar{\bar{C}}}\int_{x_{\ell_j}}^{x_{t_j}} \Delta C_p \; x \; dx$$

$$\cong -\frac{\pi}{2\bar{\bar{C}}(N+1)}\sum_{k=1}^{N+1} \Delta C_{p_k}\left(x_{\ell_j} + \frac{c_j}{2}(1 - \cos\theta_k)\right)\sin\theta_k \qquad (2.31)$$

where $\bar{\bar{C}}$ is the mean geometric chord.

According to equations (52) and (53) of ref. 31, the sectional leading edge thrust coefficient is given by:

$$c_{t_j} = \frac{\pi\sqrt{1 - M_\infty^2 \cos^2\Lambda}\,\left(w_j' - \left(\left(\frac{dz}{dx}\right)_j - \sin\alpha\right)\right)^2}{2N^2 \cos\Lambda\,(1 - M_\infty^2 + \tan^2\Lambda)} \qquad (2.32)$$

where M_∞ is the free stream Mach number, Λ the sweep angle of the leading-edge, and w_j' and $\left(\frac{dz}{dx}\right)_j$ are the induced normalwash and slope of the wing surface at the leading-edge.

The normal force coefficient is obtained by integrating the sectional normal force coefficient across the span:

$$C_N = \frac{1}{S}\int_{-\frac{b}{2}}^{\frac{b}{2}} c_n c \; dy \qquad (2.33)$$

where b is the span and S the wing area. By the transformation,

$$y = \frac{b}{4}(1 - \text{Cos}\ \phi) \tag{2.34}$$

equation (B.21) can be reduced to,

$$C_N = \frac{b}{2S}\int_o^{\pi} c_n\ c\ \text{Sin}\ \phi\ d\phi$$

$$\cong \frac{b\pi}{2SM}\sum_{i=1}^{M-1} c_{n_i} c_i\ \text{Sin}\ \phi_i \tag{2.35}$$

$$\phi_i = \frac{i}{M}\pi,\ i = 1,2,\text{---}(M-1)$$

where (M-1) is the total number of spanwise strips and the regular trapezoidal rule has been used.

Similarly the pitching moment and leading-edge thrust coefficients are given by;

$$C_M = \frac{b\pi}{2SM}\sum_{i=1}^{M-1} c_{m_i} c_i\ \text{Sin}\ \phi_i \tag{2.36}$$

ORIGINAL PAGE IS
OF POOR QUALITY

$$C_T = \frac{b\pi}{2SM}\sum_{i=1}^{M-1} c_{t_i} c_i\ \text{Sin}\ \phi_i \tag{2.37}$$

The normal force coefficient and leading-edge thrust coefficient can be resolved in the free stream direction and perpendicular to it as shown in figure 13 to obtain the lift coefficient and the induced drag coefficient:

$$C_{L_a} = C_N \text{ Cos } \alpha \tag{2.38a}$$

$$C_{D_a} = C_N \text{ Sin } \alpha \tag{2.38b}$$

$$C_{L_a} = C_T \text{ Sin } \alpha \tag{2.38c}$$

$$C_{D_b} = C_T \text{ Cos } \alpha \tag{2.38d}$$

where α is the angle of attack. Equations (2.38) can now be used to obtain the total lift and induced drag coefficients:

$$C_L = C_N \text{ Cos } \alpha + C_T \text{ Sin } \alpha \tag{2.39}$$

$$C_{D_i} = C_N \text{ Sin } \alpha - C_T \text{ Cos } \alpha \tag{2.40}$$

When the flow along the leading-edge is completely separated, the leading-edge thrust coefficient is zero.

3. Results and Discussion

It has been found during the investigation that the calculated induced velocities due to the wing become inaccurate if the control point of a free vortex segment, where induced velocities are to be evaluated, is any closer to the wing than twenty percent of the local chord. On the other hand, the induced velocities calculated above the control points of the wing show a smooth trend. Therefore, if a free vortex segment is closer than twenty percent of the local chord, the induced velocities at its control point, i.e. mid point due to the wing, are obtained by linear interpolation of the velocities calculated above four wing control points among which the point is located.

It has also been found numerically that the aerodynamic characteristics depended on the number of spanwise strips, i.e. M of equation (2.2). Therefore, a parametric study has been made to find a relation between the aspect ratio and the number of spanwise strips for reasonably accurate results (Fig. 14). It is to be noted that as the aspect ratio is decreased, the number of spanwise strips has to be increased. This is due to the fact that the spanwise variation of aerodynamic characteristics, such as pressure coefficient and thrust coefficient, is large for small aspect ratio wings. This study was performed by matching the lift coefficients obtained by using the present method to those obtained by using suction analogy (ref. 32) at one angle of attack.

The free elements of the leading-edge vortex system have been restricted not to come any closer than a minimum specified height to the wing surface, which is given empirically by,

$$Z_{min} = 0.1\ C_R \tan(22.5 - 0.5\alpha) \qquad \text{for} \quad \alpha \leq 15^\circ \qquad (2.41a)$$

$$Z_{min} = 0.1\ C_R \tan\alpha \qquad \text{for} \quad \alpha \geq 15^\circ \qquad (2.41b)$$

where C_R is the root chord and α the angle of attack. This restriction was needed because whenever the free elements are close to the wing surface, they induce large velocities on the wing and vice versa, which makes the free elements fluctuate (unstable). In the real flow, at small angles of attack, the leading-edge vortex system is weak and diffused. The present method does not account for diffused vortices and so the effect of the free vortices is artifically reduced by increasing Z_{min} as the angle of attack is decreased below 15 degrees.

All the results have been calculated by using six chordwise vortex elements on the wing; i.e., N of equation (2.1) is 6, and the length of the free vortex segments being 15 percent of the root chord. The effect of the number of chordwise vortex elements and the length of the free vortex segments is insignificant.

A computer program has been developed for the present model with the above restrictions (ref. 42). It has been used to generate aerodynamic characteristics for flat delta wings of several aspect ratios. These predicted results are compared with the available experimental data and the results by the suction analogy (ref. 32), Kandil's model (ref. 23) and Brune's model (ref. 30) as obtained by Kuhlman (ref. 33). The lift- and pitching moment-coefficients are plotted against angle of attack for complete leading-edge separation cases, i.e. zero leading-edge thrust, in figures 15 through 19. In general the agreement for the lift coefficient between the present method, suction analogy (ref. 32), Brune's model (ref. 30) and experimental data is quite good. The present method usually over-predicts the lift coefficient at small angles of attack whereas Brune's model (ref. 30) underpredicts it. For the wing of aspect ratio 0.7053, the present method becomes less accurate at high angles of attack (figure 15). This could be due to the large rate of change of pressure coefficients in spanwise directions at large angles of attack for small aspect ratio wings. A better agreement could be obtained by increasing the number of spanwise strips for small aspect ratio wings at large angles of attack. An excellent agreement is seen for the pitching moment coefficients calculated by using the present method and the experimental data in figures 16 and 17. The suction analogy can not predict accurate pitching moment coefficient because it does not calculate the surface load distribution. Although surface load distribution is predicted in Brune's model (ref. 30), the pitching moment coefficients are not predicted accurately. The pitching moment coefficients predicted by Kandil's model (ref. 25) for aspect ratio 2.0 wing are in a better agreement with experimental data than any other method, but the model is restricted up to a 20 degree angle of attack only. The effect of Mach number on the lift- and pitching moment coefficients at different angles of attack for aspect ratio 1.5 wing is shown in figure 20 and the trend for the lift coefficient agrees with that predicted by the suction analogy.

The pressure distribution for three delta wings at several angles of attack and constant x-locations are shown in figures 21 through 23. In general the pressure peak obtained by using the present method is lower than the experimental value and is shifted towards the root chord. Figure 22 shows the only comparison with the theoretical method of Brune (ref. 33) and a sharp peak is visible in Brune's model. The reason for the peak being lower in the present model is that each free vortex acts as a concentrated core by itself whereas Brune's model has a separated vortex sheet with a concentrated core at its end. Therefore, in Brune's model a sharp pressure peak will be present, whereas in the present model the pressure distribution will be more diffused.

Thus far it has been shown that the present model gives reasonable results for completely separated flow along the leading-edge. The theoretical effect of partial leading-edge separation on the aerodynamic characteristics will be shown next. Figure 24 shows the effect of varying the amount of the leading-edge suction lost on the aerodynamic characteristics for delta wing of aspect ratio 2. It can be seen from the figures that for a fixed angle of attack, the lift coefficient and the induced drag increases as the amount of the leading-edge suction lost increases. These trends are similar to the ones shown by Henderson (ref. 1). For these cases the lift is found to be highly nonlinear with angle of attack. On the other hand, a definite trend in the variation of pitching moment coefficient is not seen.

At present, the theoretical prediction of the phenomena of partial leading-edge vortex separation is not possible. The extent of the separation has been known to depend on the leading-edge geometry, the Reynolds number and the wing sweep angle (ref. 1). When the degree of partial separation can be predicted, the present method can be used to calculate the corresponding aerodynamic characteristics.

4. Conclusions and Recommendations

A theoretical method has been developed for predicting the aerodynamic characteristics of low aspect-ratio wings with partial leading-edge separation. The present method has been shown to work satisfactorily for cases with complete leading-edge vortex separation, where the leading-edge suction is zero. Some preliminary theoretical results for cases with partial leading-edge vortex separation appear to be reasonable. The method has an advantage over all previous vortex lattice methods in that the leading-edge boundary condition can be exactly satisfied. It is not restricted to incompressible flow. At the present time it is restricted to planforms with pointed wing tips only. The present method can be extended to handle arbitrary planforms at high angles of attack, as long as the vortex bursting does not occur.

The recommended topics of further research on this method are:

a. Extend the method to include the wing-tip vortices.

b. Search for a better iteration scheme for faster convergence and look for a better convergence criteria.

c. Modify the method for thick wings.

d. The method can easily be extended to complex planforms in which the inboard portion has separated flow and the outboard has attached flow.

e. The method shouldbe checked for some more cases with partial leading-edge separation.

f. The computer program coding should be made more efficient.

5. References

1. Henderson, W. P., "Effects of Wing Leading-Edge Radius and Reynolds Number on Longitudinal Aerodynamic Characteristics of Highly Swept Wing-Body Configurations at Subsonic Speeds", NASA TN D-8361, 1976.

2. Legendre, R., "E'coulement an voisinage de la pointe avant d'une aile à forte flèche aux incidences moyennes", Rechere Aéronautique (O.N.E.R.A), No. 30, pp. 3-8, 1952.

3. Adams, M. C., "Leading-Edge Separation from Delta Wings at Supersonic Speeds", Journal of the Aeronautical Sciences (Reader's Forum), Vol. 20, No. 6, June 1953.

4. Legendre, R., "E'coulement an voisinage de la pointe avant d'une aile à forte flèche aux incidences moyennes", Rechere Aéronautique (O.N.E.R.A.), No. 35, pp. 7-8, 1953.

5. Edwards, R. H., "Leading-Edge Separation from Delta Wings," Journal of the Aeronautical Sciences, Vol. 21, No. 2, Feb. 1954.

6. Brown, C. E. and Michael, W. H., "On Slender Delta Wings with Leading-Edge Separation", NACA TN 3430, 1955.

7. Mangler, K. W. and Smith, J.H.B., "A Theory of the Flow Past a Slender Delta Wing with Leading-Edge Separation", Proc. Roy. Soc. A251, pp. 200-217, 1959.

8. Smith, J.H.B., "Improved Calculation of Leading-Edge Separation for Slender, Thin, Delta Wings", Proc. Roy. Soc. A 306, pp. 67-90, 1968.

9. Smith, J.H.B., "Calculations of the Flow over Thick, Conical, Slender Wings with Leading-Edge Separation", ARC R & M 3694, 1971.

10. Gersten, K., "Calculation of Non-linear Aerodynamic Stability Derivatives of Aeroplanes", AGARD Report 342, April 1961.

11. Bollay, W., "A Non-Linear Wing Theory and Its Application to Rectangular Wings of Small Aspect Ratio", Z. Angew. Math. Mech., Bd 19, Nr. 1, pp. 21-35, Feb. 1939.

12. Garner, H. C. and Lehrian, D. E., "Non-Linear Theory of Steady Forces on Wings with Leading-Edge Separation", ARC R & M 3375, 1963.

13. Multhopp, H., "Method for Calculating the Lift Distribution of Wings (Subsonic Lifting Surface Theory)", ARC R & M 2884, 1950.

14. Sacks, A. H., Lundberg, R. E. and Hanson, C. W., "A Theoretical Investigation of the Aerodynamics of Slender Wing-Body Combinations Exhibiting Leading-Edge Separation", NASA CR-719, 1967.

15. Lawrence, H. R., "The Lift Distribution on Low Aspect Ratio Wings at Subsonic Speeds", J. Aeron. Sci., Vol. 18, No. 10, Oct. 1951.

16. Nangia, R. K. and Hancock, G. J., "A Theoretical Investigation for Delta Wings with Leading-Edge Separation at Low Speeds", ARC CP-1086, 1968.

17. Polhamus, E. C., "A Concept of the Vortex Lift of Sharp-Edge Delta Wings Based on a Leading-Edge-Suction Analogy", NASA TN D-3767, 1966.

18. Polhamus, E. C., "Charts for Predicting the Subsonic Vortex-Lift Characteristics of Arrow, Delta and Diamond Wings", NASA TND-6243, 1971.

19. Lamar, J. E., "A Modified Multhopp Approach for Predicting Lifting Pressures and Camber Shape for Composite Planforms in Subsonic Flow", NASA TN D-4427, 1968.

20. Snyder, M. H. and Lamar, J. E., "Application of the Leading-Edge-Suction Analogy to Prediction of Longitudinal Load Distribution and Pitching Moments for Sharp-Edged Delta Wings", NASA TN D-6994, 1972.

21. Mook, D. T. and Maddox, S. A., "Extension of a Vortex-Lattice Method to Include the Effects of Leading-edge Separation", Journal of Aircraft, Vol. 11, pp. 127-128, Feb. 1974.

22. Giesing, J. P., Kalman, T. P. and Rodden, W. P., "Subsonic Unsteady Aerodynamics for General Configurations; Direct Application of the Non-planar Doublet-Lattice Method", USAF FDL-TR-71-5, 1971.

23. Kandil, O. A., Mook, D. T. and Nayfeh, A. H., "Nonlinear Prediction of the Aerodynamic Loads of Lifting Surfaces", AIAA Paper No. 74-503, 1974.

24. Belotserkovskii, S. M., "Calculation of Flow Around Wing of Arbitrary Planform Over a Wide Range of Angles of Attack", Mekhanika Zhidkosti i Gaza, Vol. 3, No. 4, pp. 32-44, 1968, Translated in Fluid Dynamics, Consultants Bureau, pp. 20-27.

25. Kandil, O. A., Mook, D. T. and Nayfeh, A. H., "Subsonic Loads on Wings Having Sharp Leading-Edges and Tips", Journal of Aircraft, Vol. 13, No. 1, pp. 62-63, 1976.

26. Kandil, O. A., Mook, D. T. and Nayfeh, A. H., "New Convergence Criteria for the Vortex-Lattice Models of the Leading-Edge Separation", NASA SP-405, 1976.

27. Rehbach, C., "Calculation of Flows Around Zero Thickness Wings with Evolutive Vortex Sheets", NASA TTF-15183, 1973.

28. Rehbach, C., "Numerical Investigation of Vortex Sheets Issuing from a Separation Line Near the Leading-Edge", NASA TTF-15530, 1974.

29. Nathman, J. K., "Delta Wings in Incompressible Flows", AIAA Paper No. 77-320, 1977.

30. Brune, G. W., Weber, J. A., Johnson, F. T., Lu, P. and Rubbert, P. E., "A Three Dimensional Solution of Flow over Wings with Leading-Edge Separation, Part I - Engineering Document", NASA CR-132709, 1975.

31. Lan, C. E., "A Quasi-Vortex-Lattice Method in Thin Wing Theory", Journal of Aircraft, Vol. 11, No. 9, pp. 518-527, Sept. 1974.

32. Lamar, J. E. and Gloss, B. B., "Subsonic Aerodynamic Characteristics of Interacting Lifting Surfaces with Separated Flows around Sharp Edges Predicted by a Vortex Lattice Method", NASA TN D-7921, 1975.

33. Kuhlman, J., "Load Distributions on Slender Delta Wings having Vortex Flow", Journal of Aircraft, Vol. 14, No. 7, pp. 699-702, July 1977.

34. Fink, P. T., "Wind-Tunnel Tests on a Slender Delta Wing at High Incidence", Z. Flugwissenschaften, Jahrg. 4, Heft 7, pp. 247-249, July 1956.

35. Peckham, D. H., "Low-Speed Wind-Tunnel Tests on a Series of Uncambered Slender Pointed Wings with Sharp Edges", ARC R & M 3186, 1961.

36. Tosti, L. P., "Low-Speed Static Stability and Damping-in-Roll Characteristics of Some Swept and Unswept Low Aspect Ratio Wings", NACA TN 1468, 1947.

37. Wentz, W. H., "Effects of Leading-Edge Camber on Low-Speed Characteristics of Slender Delta Wings", NASA CR-2002, 1972.

38. Bartlett, G. E. and Vidal, R. J., "Experimental Investigation of Influence of Edge Shape on the Aerodynamic Characteristics of Low Aspect Ratio Wings at Low-Speeds", Journal of the Aeronautical Sciences, Vol. 22, No. 8, pp. 517-533, Aug. 1955.

39. Fink, P. T. and Taylor, J., "Some Low-Speed Experiments with 20 deg. Delta Wings", ARC R & M 3489, 1967.

40. Marsden, D. J., Simpson, R. W. and Rainbird, W. J., "The Flow over Delta Wings at Low Speeds with Leading-Edge Separation", The College of Aeronautics, Cranfield, Rept. No. 114, Feb. 1958.

41. Butler, D. J. and Hancock, G. J., "A Numerical Method for Calculating the Trailing Vortex System behind a Swept Wing at Low Speed", The Aeron. J. of the Royal Aeronautical Society, Vol. 75, pp. 564-568, Aug. 1971.

42. Mehrotra, S. C., "A Theoretical Investigation of the Aerodynamics of Low Aspect-Ratio Wings with Partial Leading-Edge Separation - A Computer Program", University of Kansas Report CRINC-FRL-266-2, 1978.

6. Appendices

6.1 Appendix A: Evaluation of Induced Velocity Due to a Line Vortex-Segment

In the linearized compressible flow the velocity field induced by a line vortex segment of strength Γ (figure 12) is given by (ref. 31),

$$\vec{V}(\vec{R}) = \frac{\beta^2\Gamma}{4\pi} \int_\ell \frac{(\vec{R}_\ell - \vec{R}) \times d\vec{\ell}}{R_\beta^3} \tag{A.1}$$

where

$$\beta = \sqrt{1 - M^2}, \; \vec{R} = x\vec{i} + y\vec{j} + z\vec{k}$$

$$\vec{R}_\ell = \xi\vec{i} + \eta\vec{j} + \zeta\vec{k}$$

$$\vec{R}' = x\vec{i} + \beta y\vec{j} + \beta z\vec{k}$$

$$\vec{R}'_\ell = \xi\vec{i} + \beta\eta\vec{j} + \beta\zeta\vec{k}$$

$$R_\beta = [(\xi-x)^2 + \beta^2(\eta-y)^2 + \beta^2(\zeta-z)^2]^{1/2}$$

$$= |\vec{R}'_\ell - \vec{R}'|$$

The substitution $\vec{R}_\ell - \vec{R} = \vec{a} + \tau\vec{\ell}$, reduces equation (A.1) to,

$$\vec{V}(\vec{R}) = \frac{\beta^2\Gamma}{4\pi} \; \vec{a} \times \vec{\ell} \int_0^1 \frac{d\tau}{(\bar{A}\tau^2 + \bar{B}\tau + \bar{C})^{3/2}}$$

$$= \frac{\beta^2\Gamma}{4\pi} \; \vec{a} \times \vec{\ell} \; \{\frac{2\,\bar{B}}{(\bar{B}^2 - 4\bar{A}\,\bar{C})\bar{C}^{1/2}}$$

$$- \frac{2(2\,\bar{A} + \bar{B})}{(\bar{B}^2 - 4\bar{A}\bar{C})(\bar{A} + \bar{B} + \bar{C})^{1/2}}\}, \; \bar{B}^2 - 4\bar{A}\bar{C} \neq 0 \qquad (A.2)$$

where $\bar{A} = |\vec{\ell}'|^2$, $\bar{B} = 2\vec{a}' \cdot \vec{\ell}'$ and $\bar{C} = |\vec{a}'|^2$. Further, it can be shown that (ref. 31),

$$\bar{B}^2 - 4\bar{A}\bar{C} = -4|\vec{a}' \times \vec{\ell}'|^2 \qquad (A.3)$$

$$2\bar{A} + \bar{B} = 2\,\vec{b}' \cdot \vec{\ell}' \qquad (A.4)$$

$$\bar{A} + \bar{B} + \bar{C} = |\vec{b}'|^2 \qquad (A.5)$$

where

$$\vec{a} = (x_1 - x)\vec{i} + (y_1 - y)\vec{j} + (z_1 - z)\vec{k}$$

$$\vec{b} = (x_2 - x)\vec{i} + (y_2 - y)\vec{j} + (z_2 - z)\vec{k}$$

$$\vec{\ell} = (x_2 - x_1)\vec{i} + (y_2 - y_1)\vec{j} + (z_2 - z_1)\vec{k}$$

$$\vec{a}' = (x_1 - x)\vec{i} + \beta(y_1 - y)\vec{j} + \beta(z_1 - z)\vec{k}$$

$$\vec{b}' = (x_2 - x)\vec{i} + \beta(y_2 - y)\vec{j} + \beta(z_2 - z)\vec{k}$$

$$\vec{\ell}' = (x_2 - x_1)\vec{i} + \beta(y_2 - y_1)\vec{j} + \beta(z_2 - z_1)\vec{k}$$

On rearranging, equation (A.2) becomes

$$\vec{V}(\vec{R}) = \frac{\beta^2\Gamma}{4\pi} \frac{\vec{a} \times \vec{\ell}}{|\vec{a}' \times \vec{\ell}'|^2} \left\{\frac{\vec{b}'}{|\vec{b}'|} - \frac{\vec{a}'}{|\vec{a}'|}\right\} \cdot \vec{\ell}' \qquad (A.6)$$

6.2 Appendix B: Derivation of Expressions for Pressure Distribution

Consider two adjoining sets of spanwise strips of bound elements (Sketch B.1). Along the common edge, there are three trailing vortices: one due to right set of bound elements, one due to the left set of bound elements and the other due to the leading-edge vortex system. The force acting on the chordwise element of length Δx of the leading-edge vortex system is, by the Kutta-Joukowski theorem,

$$F_{L_i} = \rho V_\infty^2 \Gamma_j v_i \Delta x \tag{B.1}$$

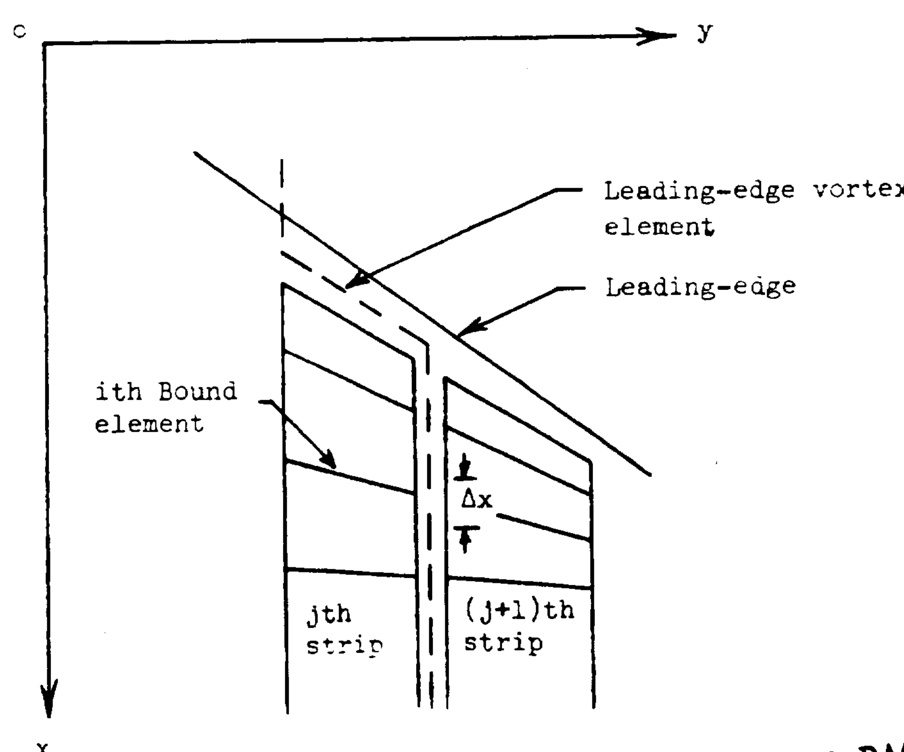

Sketch B.1

where ρ is the fluid density, V_∞ the free stream velocity, Γ_j the strength of jth leading-edge vortex element and v_i the sidewash at point i. It follows that the force acting at ith point per unit dynamic pressure and length is,

$$\left(\frac{F_{L_i}}{q\Delta x}\right) = 2\Gamma_j v_i \tag{B.2}$$

where $q = \frac{1}{2}\rho V_\infty^2$, the dynamic pressure. A similar expression for the force per unit dynamic pressure and length can be written for the outside leg of the jth strip as,

$$\left(\frac{F_{N_i}}{q\Delta x}\right)_R = -2v_i \int^{x_i} \gamma \, dx \tag{B.3}$$

where γ is the bound vortex density x_ℓ the leading-edge x-coordinate of the trailing-leg under consideration. The transformation,

$$x = x_\ell + \frac{c_j}{2}(1 - \text{Cos } \theta) \tag{B.4}$$

reduces equation (B.3) to the form,

$$\left(\frac{F_{N_i}}{q\Delta x}\right)_R = - v_i c_j \int_o^{\theta_i} \gamma \text{ Sin } \theta \, d\theta$$

$$\cong - \frac{\pi c_j v_i}{N}\left[\sum_{k=1}^{i-1} \gamma_k \text{ Sin } \theta_k + \frac{\gamma_i \text{ Sin } \theta_i}{2}\right]_R \tag{B.5}$$

where c_j is the local chord, N the number of bound elements in chordwise direction and $\theta_k = \frac{(2k - 1)}{2N} \pi$. The integral has been reduced to a finite sum through the regular trapezoidal rule. Similarly, for the left leg of (j+1)th strip,

$$\left(\frac{F_{N_i}}{q\Delta x}\right)_L = \frac{\pi\, c_j v_i}{N} \left[\sum_{k=1}^{i-1} \gamma_k \,\text{Sin}\,\theta_k + \frac{\gamma_i \,\text{Sin}\,\theta_i}{2}\right]_L \tag{B.6}$$

Therefore, the force per unit dynamic pressure and per unit length at the ith point is given by the sum of equations (B.2), (B.5) and (B.6).

$$\left(\frac{F_i}{q\Delta x}\right) = \left(\frac{F_{L_i}}{q\Delta x}\right) + \left(\frac{F_{N_i}}{q\Delta x}\right)_R + \left(\frac{F_{N_i}}{q\Delta x}\right)_L \tag{B.7}$$

Equation (B.7) is evaluated at all endpoints of wing bound elements and linear interpolation is performed to obtain the force acting at the control station which is inside the vortex strip. Let it be denoted by $H_{j,i}$ for ith bound element of jth strip. Then, the contribution to differential pressure coefficient, ΔC_p, due to the chordwise vortices is,

$$\left(\Delta C_{p_{j,i}}\right)_T = \frac{H_{j,i}}{\Delta y_j} \tag{B.8}$$

where Δy_j is the width of jth spanwise strip.

Contribution to ΔC_p due to bound elements is calculated in the following manner. The normal force per unit length acting at ith

ORIGINAL PAGE IS
OF POOR QUALITY

bound element of jth strip (Sketch B.2) is,

$$F_{B_{j,i}} = \rho V_\infty^2 \, (u_i\gamma_i \text{ Cos } \psi_i - v_i\gamma_i \text{ Sin } \psi_i) \frac{\Delta y_i}{\text{Cos } \psi_i}$$

or

$$F_{B_{j,i}} = 2q(u_i - v_i \tan \psi_i)\gamma_i \Delta y_j \qquad (B.9)$$

where γ_i is the bound vortex density, u_i and v_i the x and y components of the velocity, ψ_i the sweep angle of the bound elements and Δy_j the width of the jth strip. It follows that the ΔC_p due to the ith bound element is given by dividing equation (B.9) by $(q\Delta y_j)$;

$$\left(\Delta C_{p_{j,i}}\right)_B = 2(u_i - v_i \tan \psi_i)\gamma_i \qquad (B.10)$$

The total ΔC_p is given as the sum equations (B.8) and (B.10):

$$\Delta C_{p_{j,i}} = \left(\Delta C_{p_{j,i}}\right)_T + \left(\Delta C_{p_{j,i}}\right)_B \qquad (B.11)$$

Up to this point ΔC_p has been calculated at the regular wing vortex locations. The contribution from the leading-edge vortex element on the planform near the leading-edge (EF in figure 11) has yet to be considered. This is done in two steps; 1. Extrapolate ΔC_p due to the wing vortex system to obtain the ΔC_p at the location of the leading-edge vortex element EF; and 2. Subtract ΔC_p induced by the leading-edge vortex element.

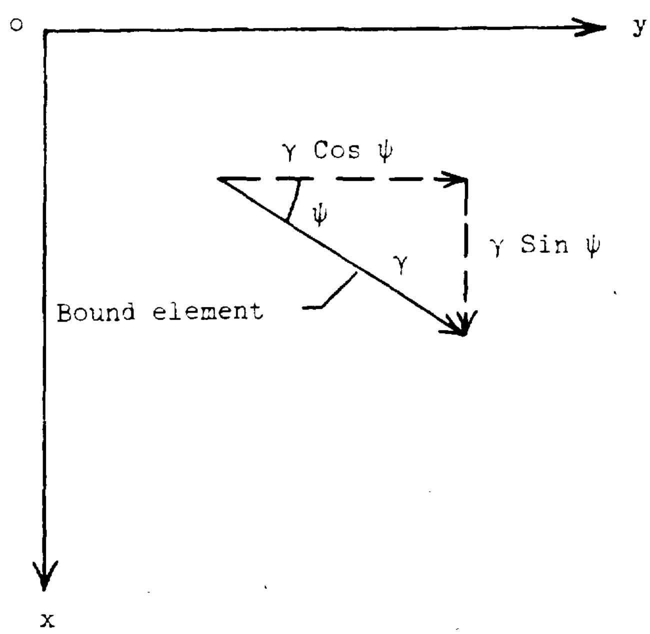

Sketch B.2

To obtain ΔC_p at any chordwise location, $\Delta C_p \sin\theta$ will be Fourier-analyzed. The factor, Sin θ, is included to eliminate the known square root singularity of ΔC_p at the leading and trailing edges. Therefore, let

$$\Delta C_p \text{ Sin } \theta = a_o + \sum_{=1}^{N} a_\ell \text{ Cos } \ell\theta \qquad \text{(B.12)}$$

where,

$$a_o = \frac{1}{\pi} \int_o^\pi \Delta C_p \text{ Sin } \theta \, d\theta$$

$$\cong \frac{1}{N} \sum_{k=1}^{N} \Delta C_{p_k} \text{ Sin } \theta_k$$

$$a_\ell = \frac{2}{\pi} \int_0^\pi \Delta C_p \text{ Sin } \theta \text{ Cos } \ell\theta \, d\theta$$

$$\cong \frac{2}{N} \sum_{k=1}^{N} \Delta C_{p_k} \text{ Sin } \theta_k \text{ Cos } \ell\theta_k$$

$$\theta_k = \frac{(2k - 1)}{2N} \pi, \; k = 1,2,\text{------}N$$

N - Number of chordwise lines

The integrals for Fourier coefficients are reduced to finite sums through the mid-point trapezoidal rule. Equation (B.12) can now be used to calculate ΔC_p at the location of the leading-edge vortex element EF, which is located at $\theta = \pi/2(N + 1)$. To achieve the second step mentioned above, the constant vorticity of the leading-edge vortex element is first converted to vortex density. The concentrated vorticity is related to vortex density by,

$$\Gamma = \int \gamma \, dx \tag{B.13}$$

On using equation (B.4) in the above equation,

$$\Gamma_j = \frac{c_j}{2} \int \gamma \text{ Sin } \theta \, d\theta \tag{B.14}$$

Assuming that the concentrated vorticity due to leading-edge vortex system is distributed near the leading-edge only and using the mid-point trapezoidal rule, the equation (B.14) reduces to:

$$\Gamma_j = \frac{\pi c_j}{2(N + 1)} \gamma_j \text{ Sin } \theta_1$$

or

$$\gamma_j = \frac{2(N + 1)}{\pi \ c_j \text{ Sin } \theta_1} \Gamma_j \tag{B.15}$$

where $\theta_1 = \pi/2\ (N + 1)$. Therefore, the decrease in ΔC_p value at the leading-edge vortex element is given by using equation (B.10) as,

$$(\Delta C_p)_{\text{decrease}} = - (u - v \tan \psi)_{\ell e}\ \gamma_j \tag{B.16}$$

where the subscript ℓe means that the variables u, v and ψ are evaluated at the leading-edge vortex element. Note that this decrease in ΔC_p value near the leading-edge from the usual ΔC_p distribution is a result of the leading-edge Kutta condition. Hence, the equations (B.12) and (B.14) can be used to calculate the actual ΔC_p at the location of the leading-edge vortex elements.

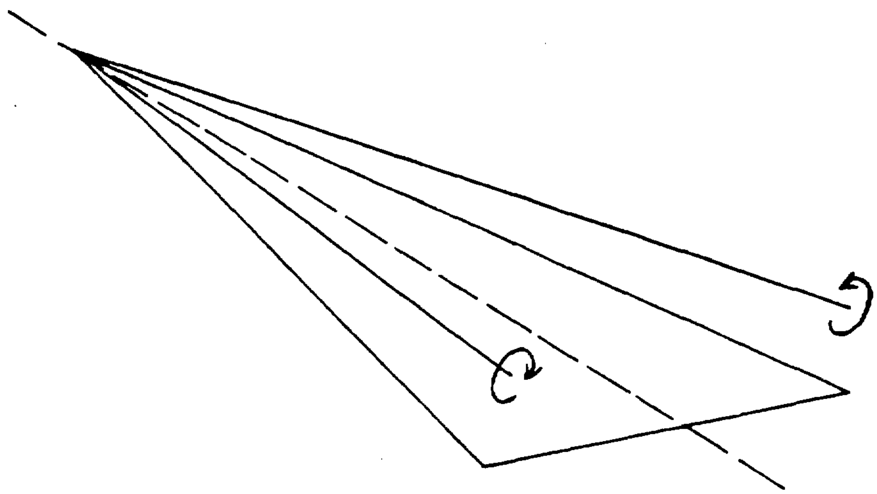

Figure 1. Legendre's model

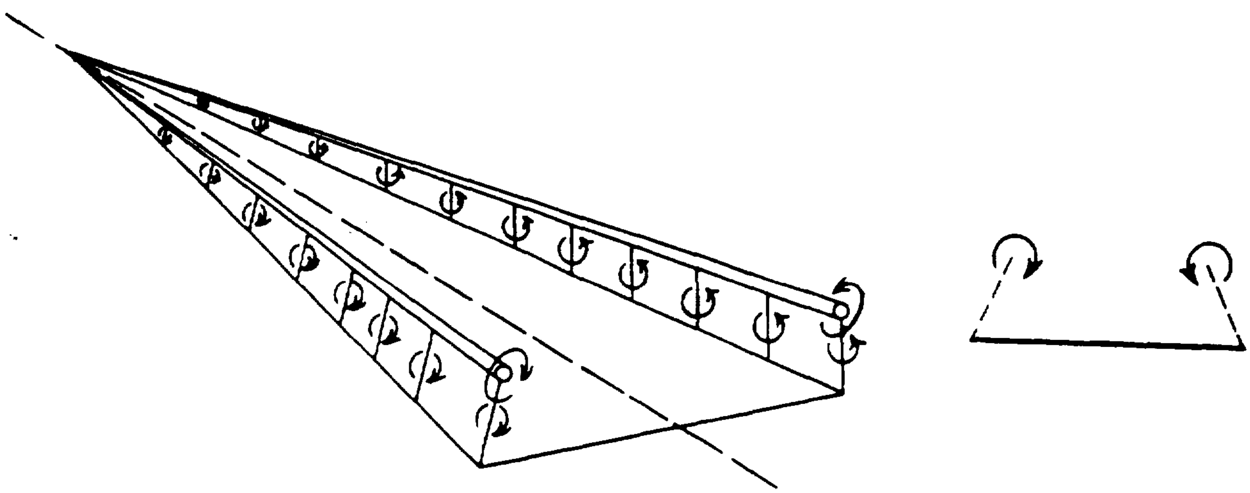

Figure 2. Brown and Michael's model

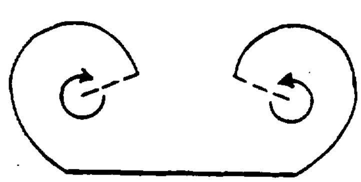

Figure 3. Mangler and Smith's model

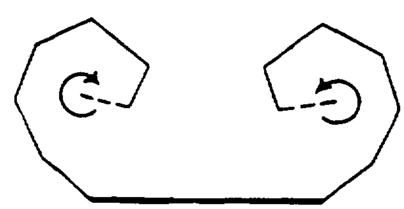

Figure 4. Smith's model

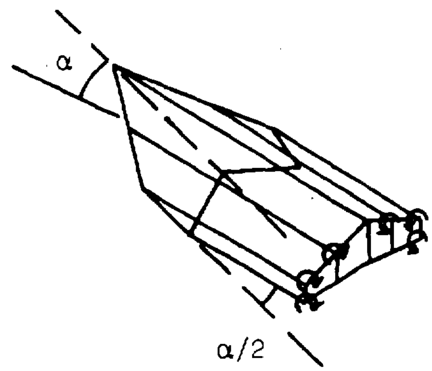

Figure 5. Gersten's model

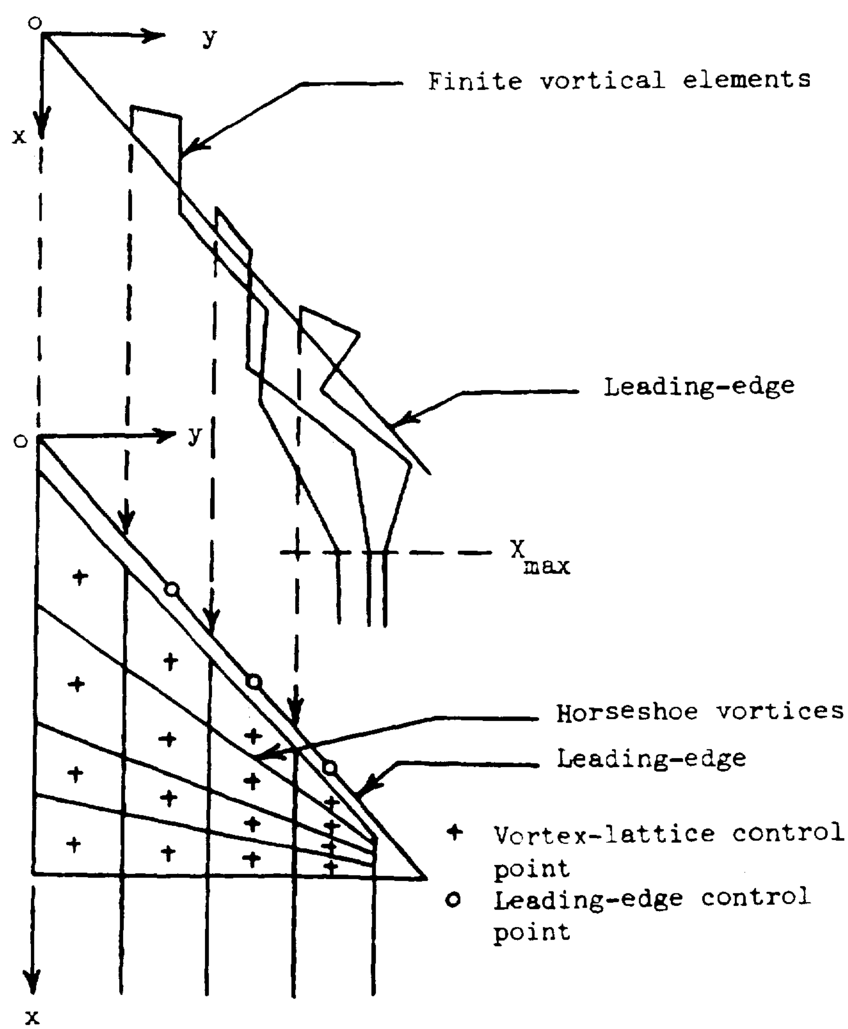

Figure 6. Mook and Maddox model

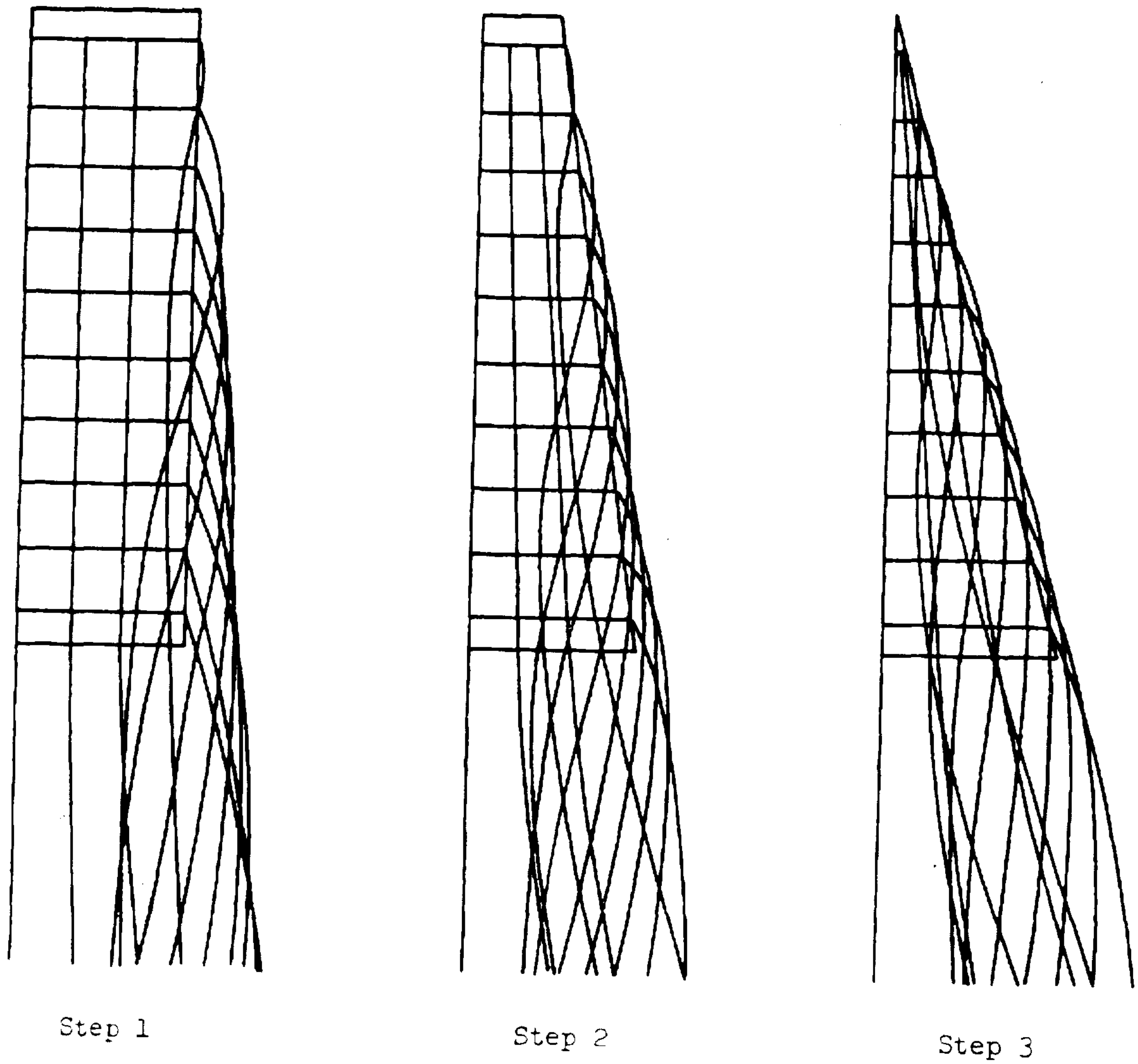

Figure 7. Rehbach's model

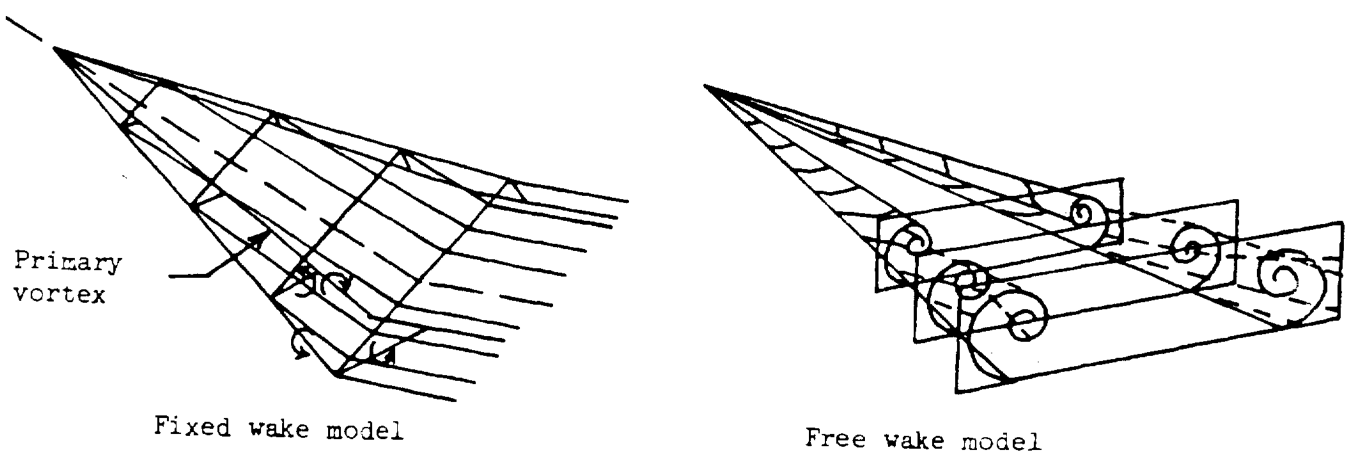

Figure 8. Nathman's models

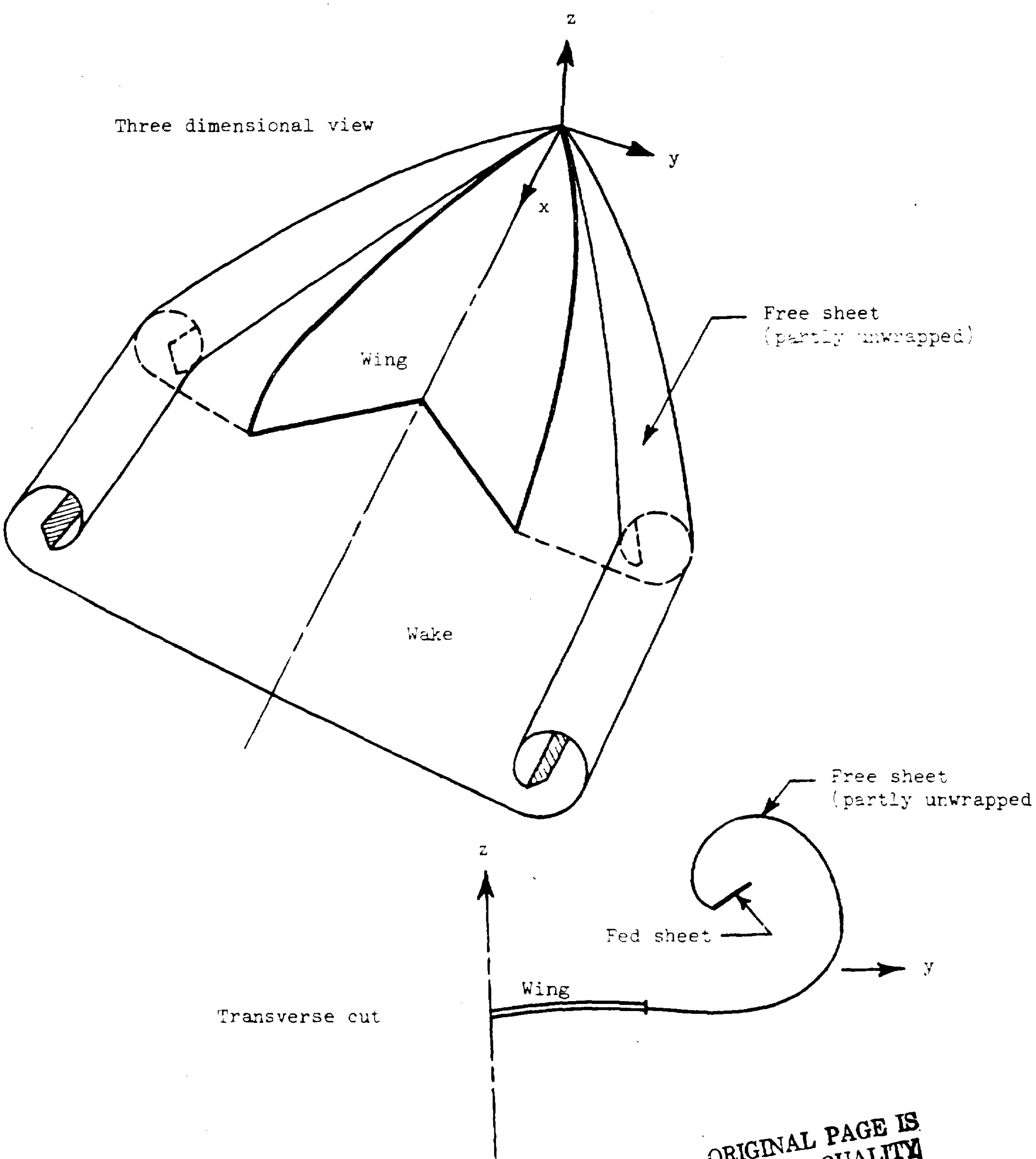

Figure 9. Brune's model

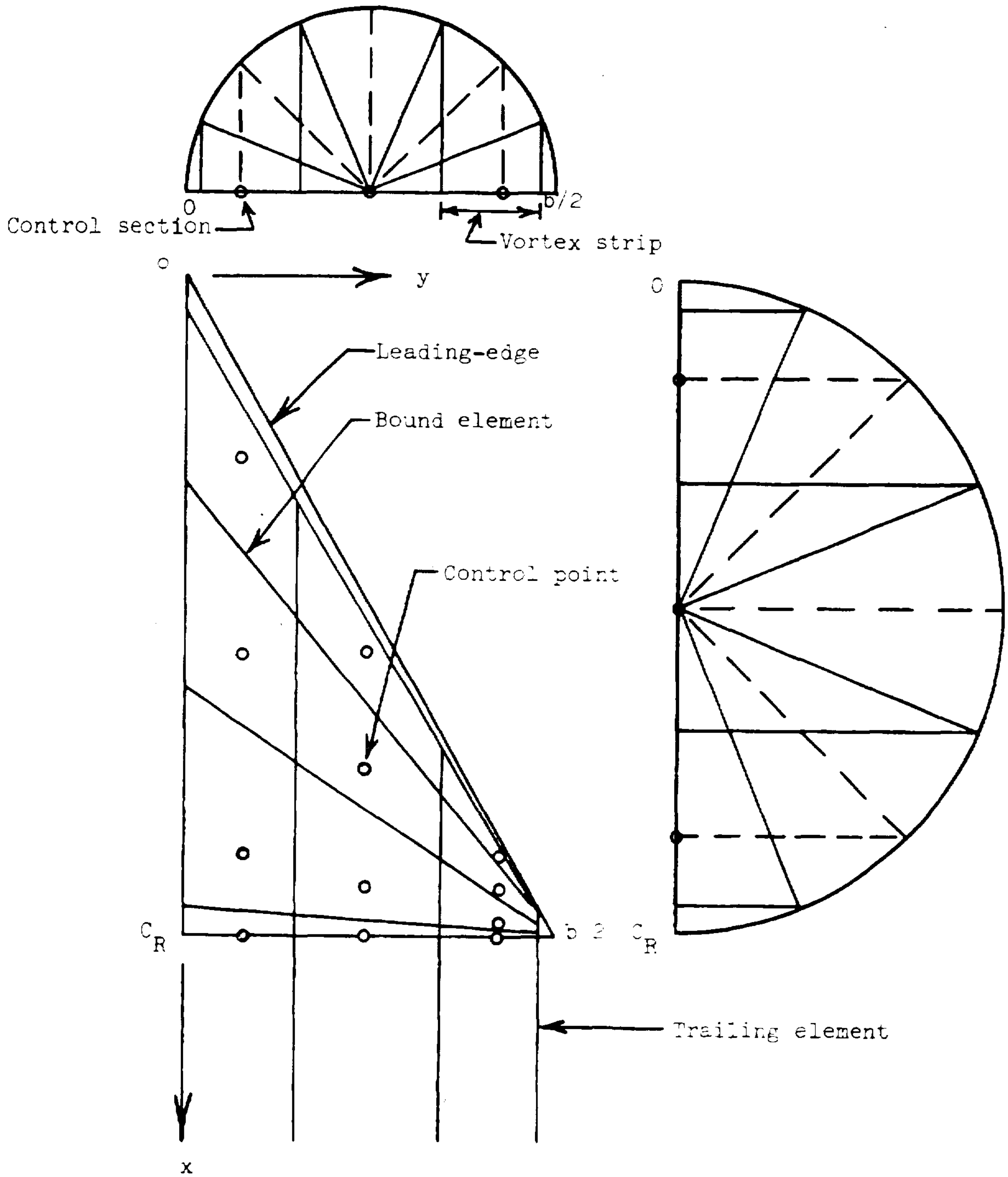

Figure 10. Wing geometry without leading-edge vortex system

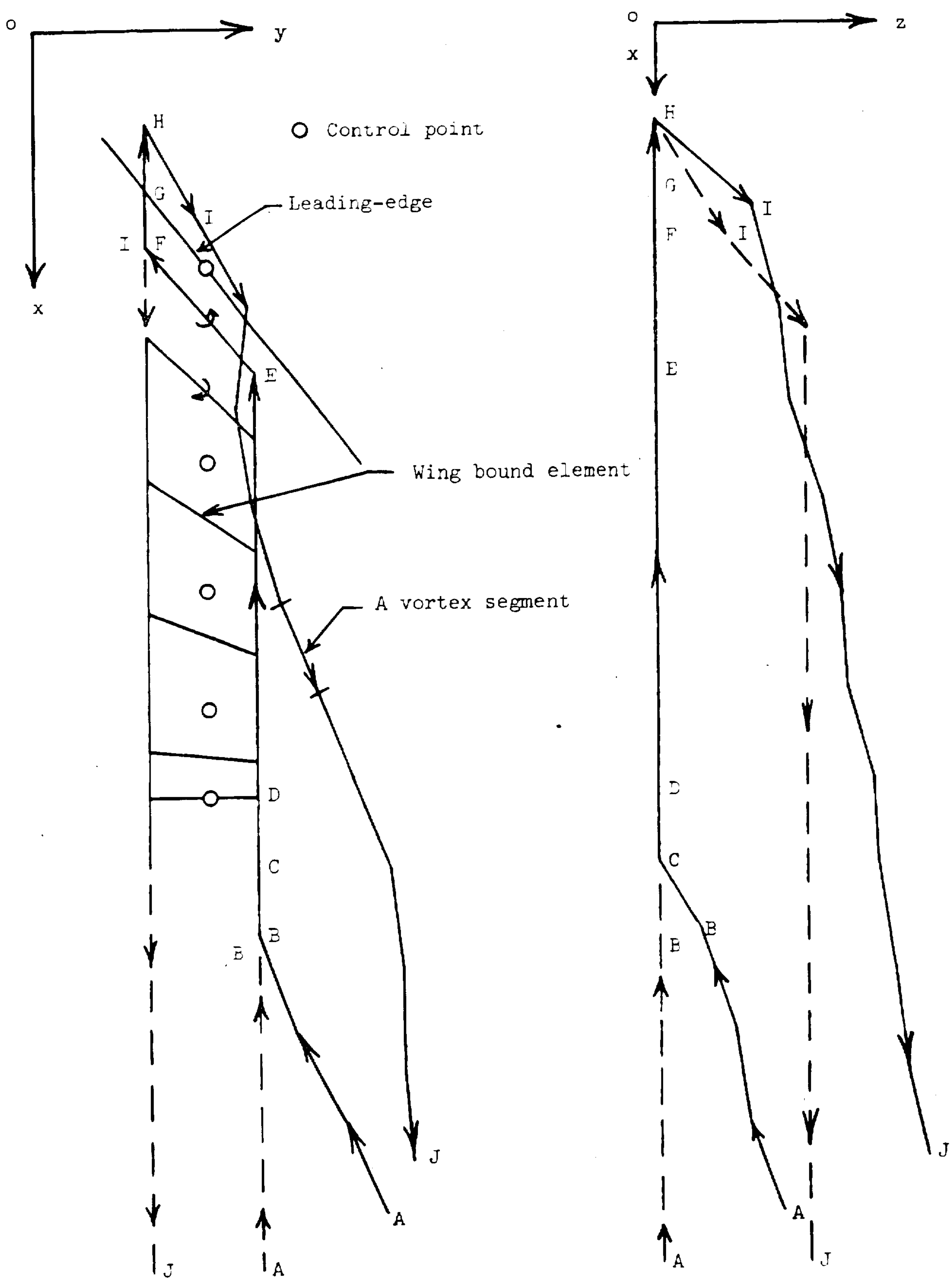

Figure 11. A typical vortex element of leading-edge vortex system

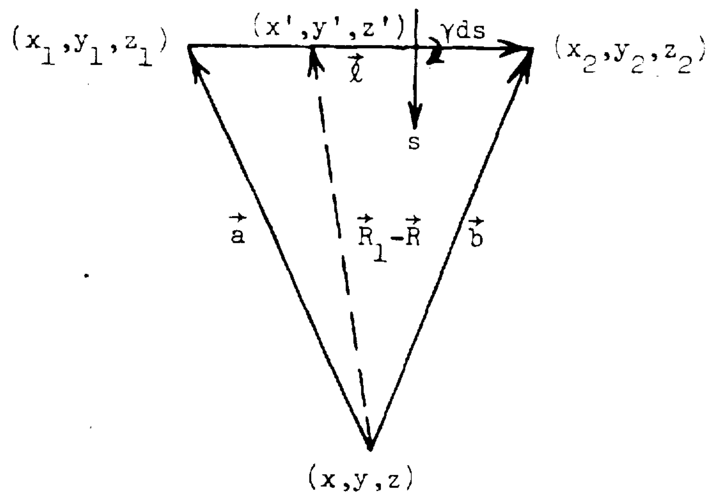

Figure 12. Vortex segment geometry

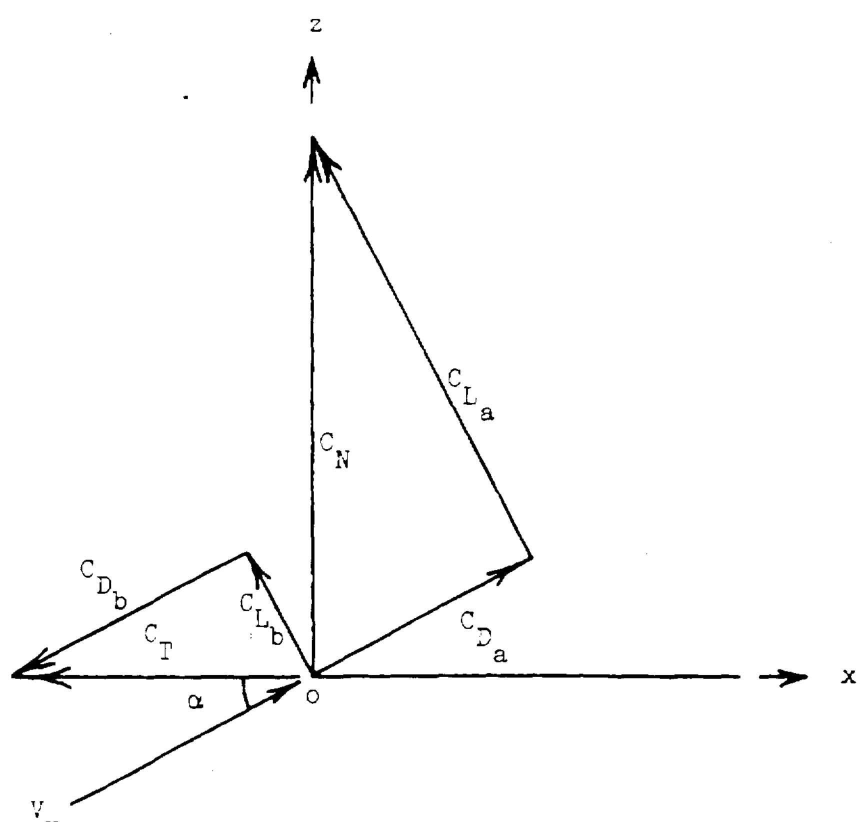

Figure 13. Resolution of forces

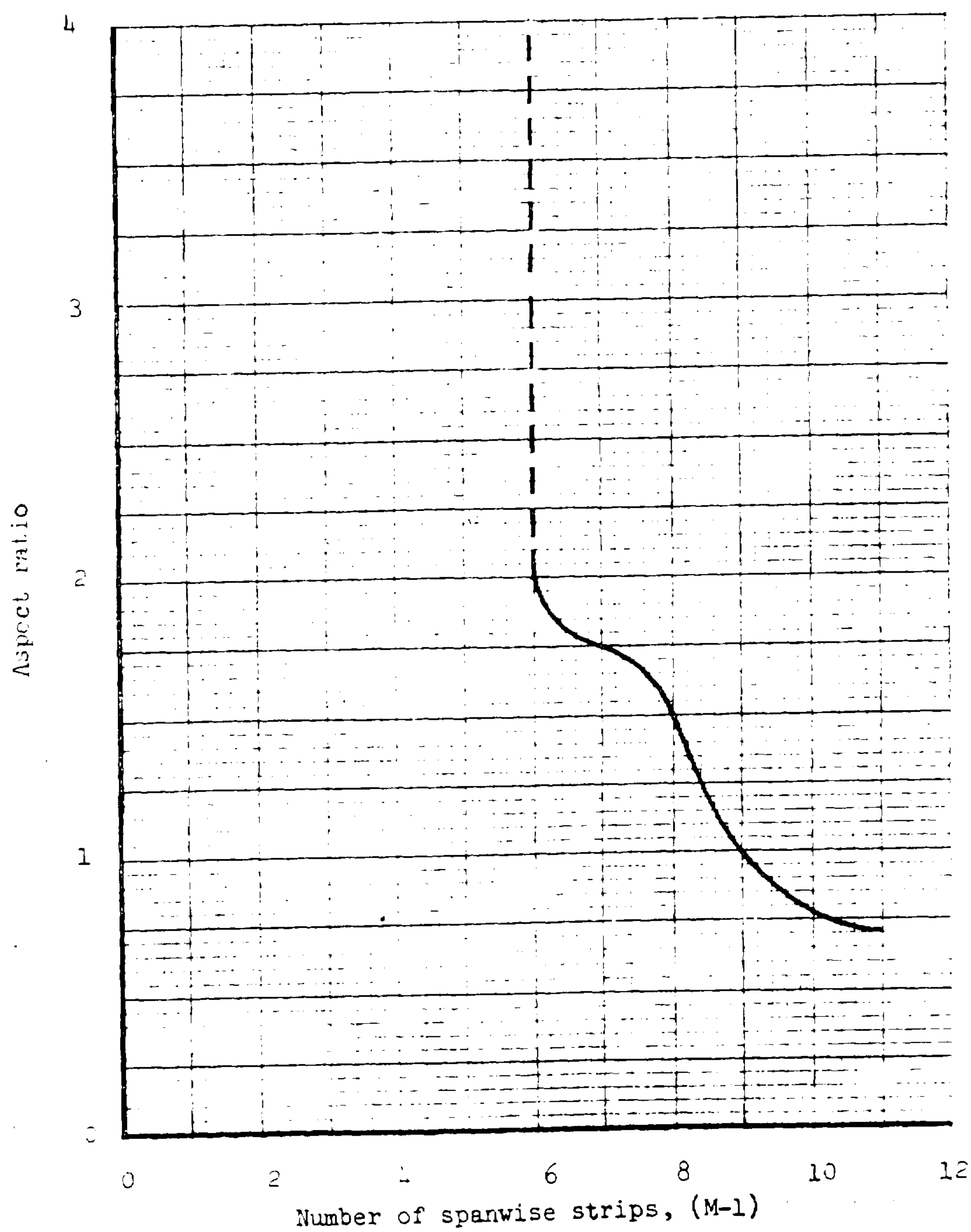

Figure 14. Variation of number of spanwise strips with aspect ratio

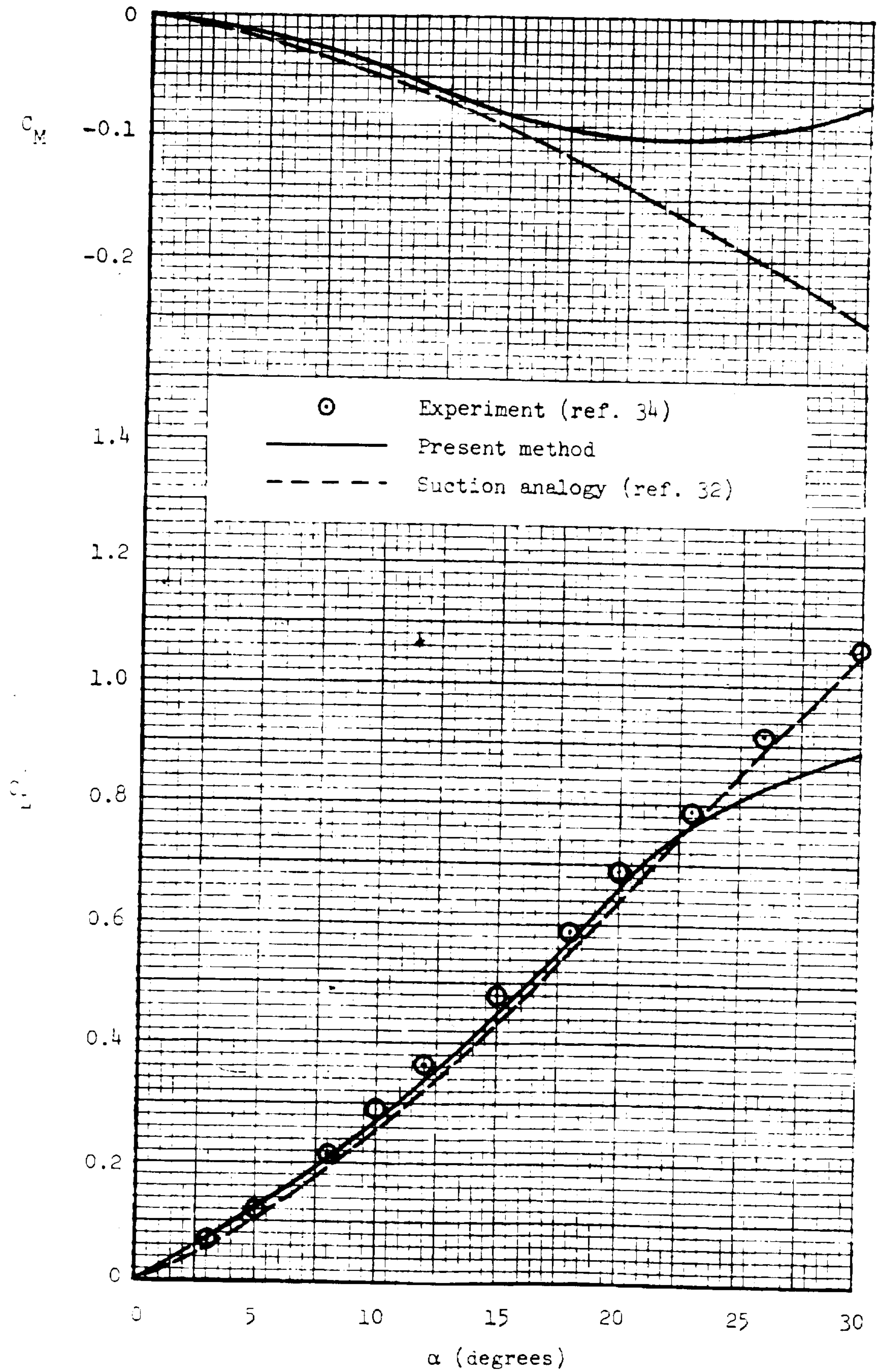

Figure 15. Variation of lift and pitching moment (about $0.25\bar{C}$) coefficients with angle of attack for aspect ratio 0.7053 delta wing

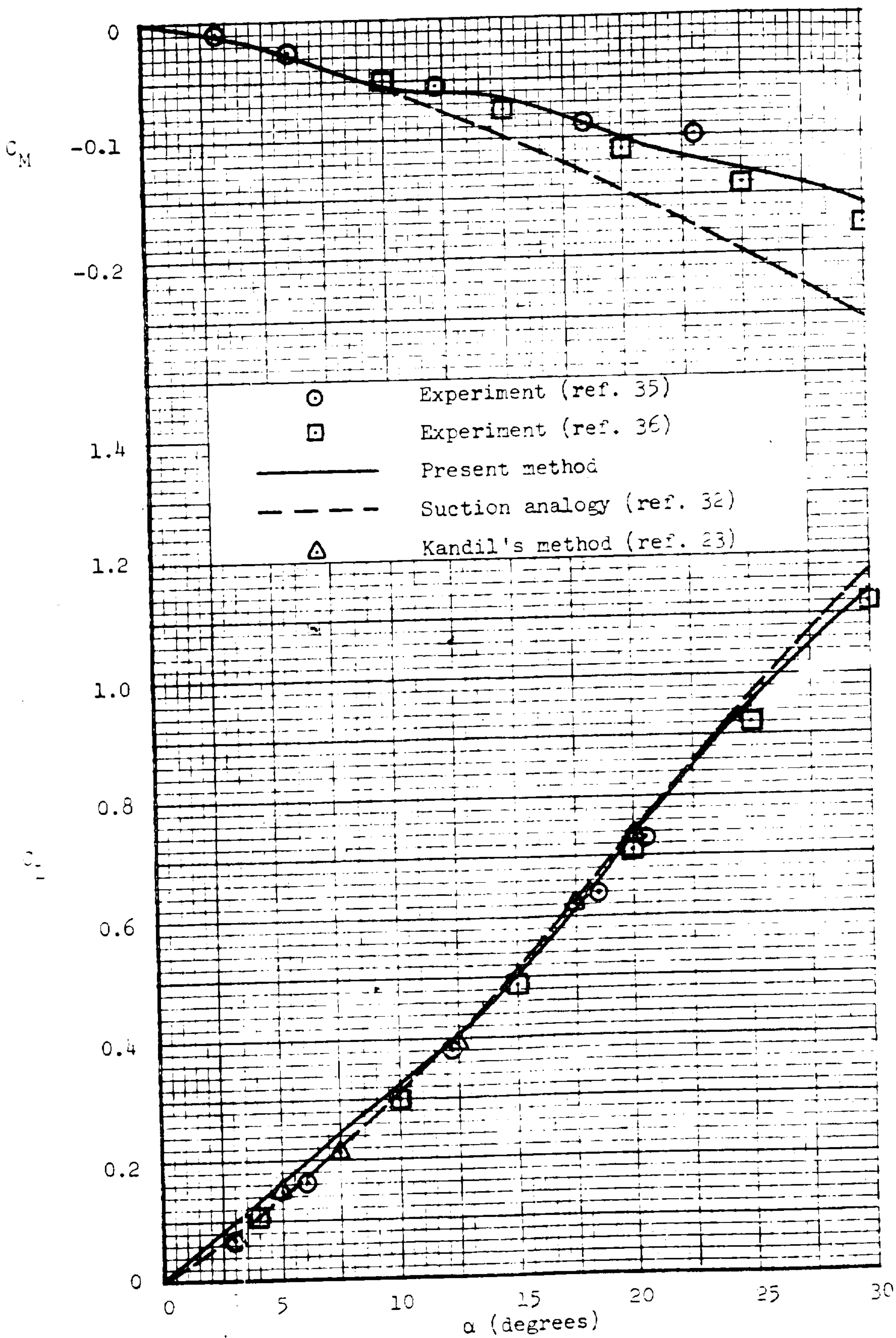

Figure 16. Variation of lift and pitching moment (about $0.25\bar{c}$) coefficients with angle of attack for aspect ratio 1.0 delta wing

ORIGINAL PAGE IS OF POOR QUALITY

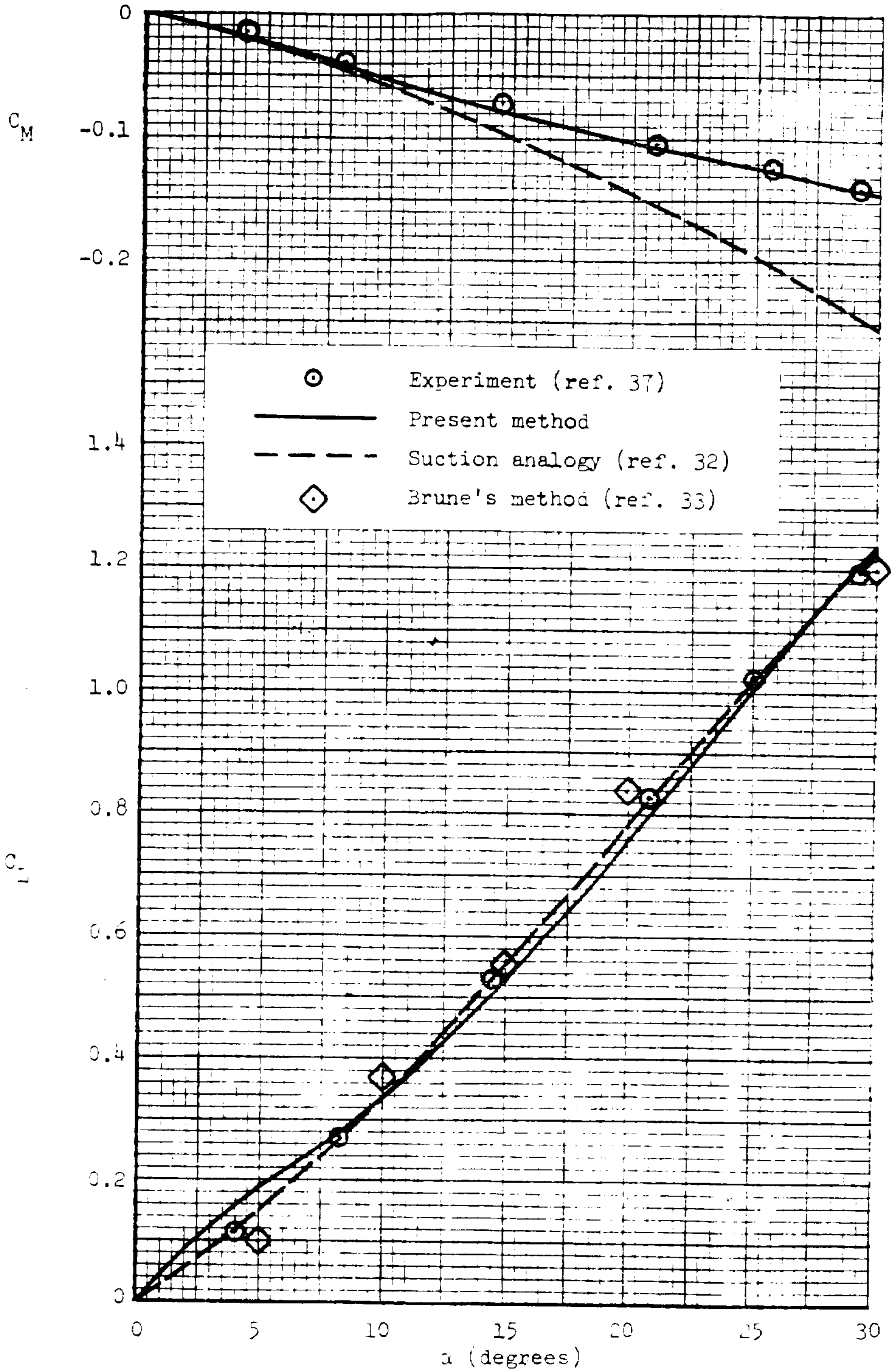

Figure 17. Variation of lift and pitching moment (about 0.[illegible]5$\bar{c}$) coefficients with angle of attack for aspect ratio 1.147 delta wing

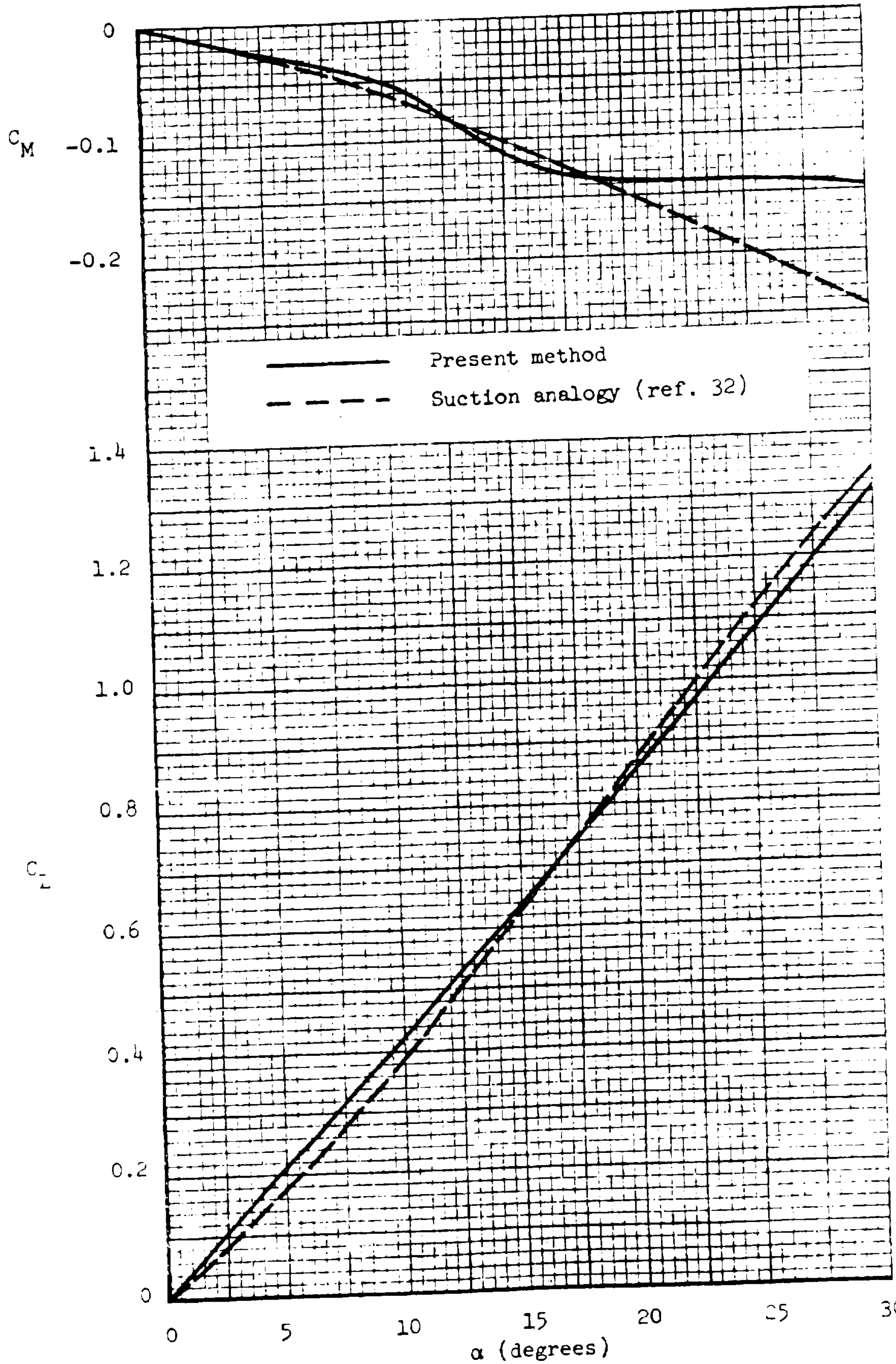

Figure 18. Variation of lift and pitching moment (about $0.25\bar{c}$) coefficients with angle of attack for aspect ratio 1.4559 delta wing

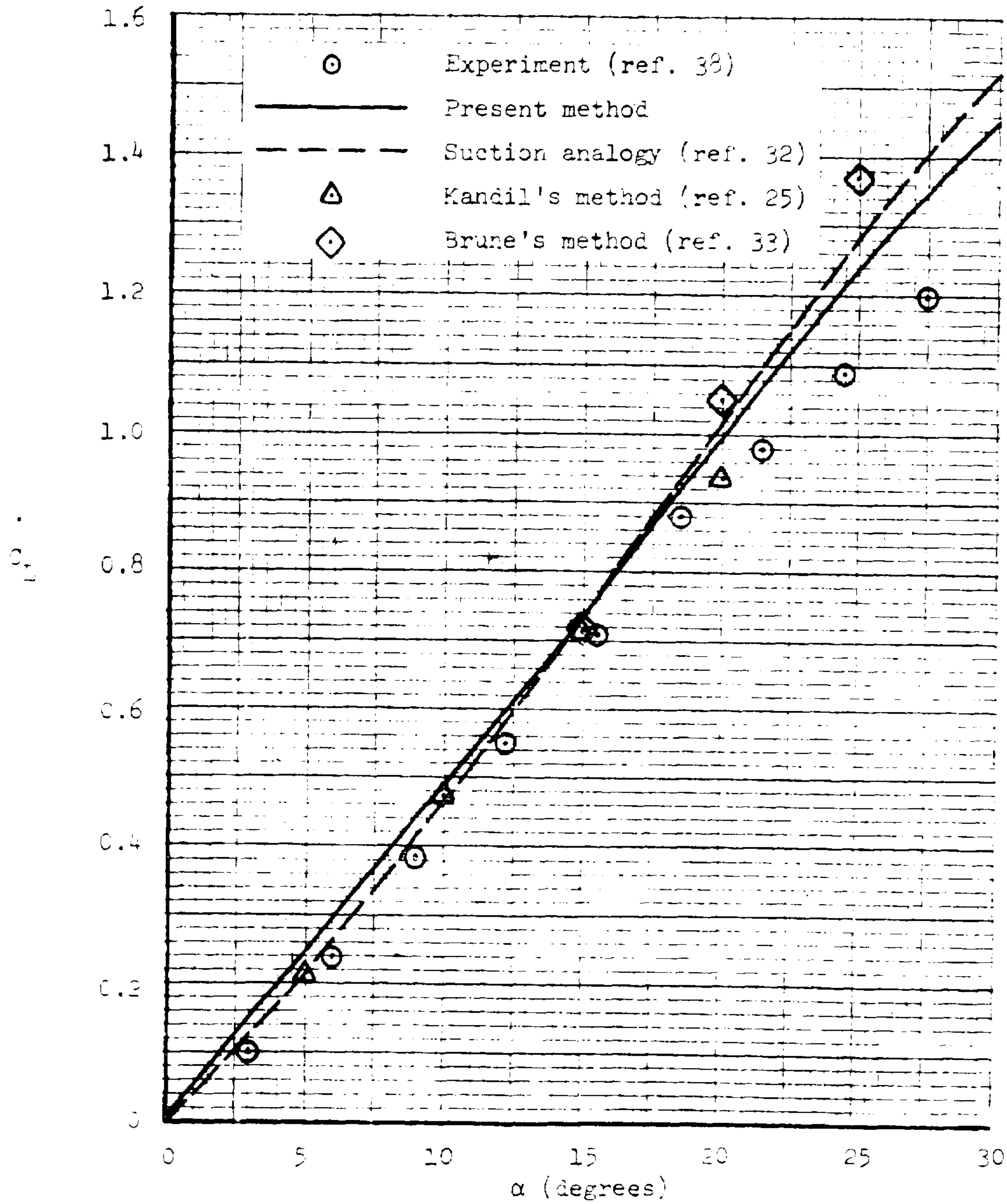

Figure 19a. Variation of lift coefficient with angle of attack for aspect ratio 2.0 delta wing

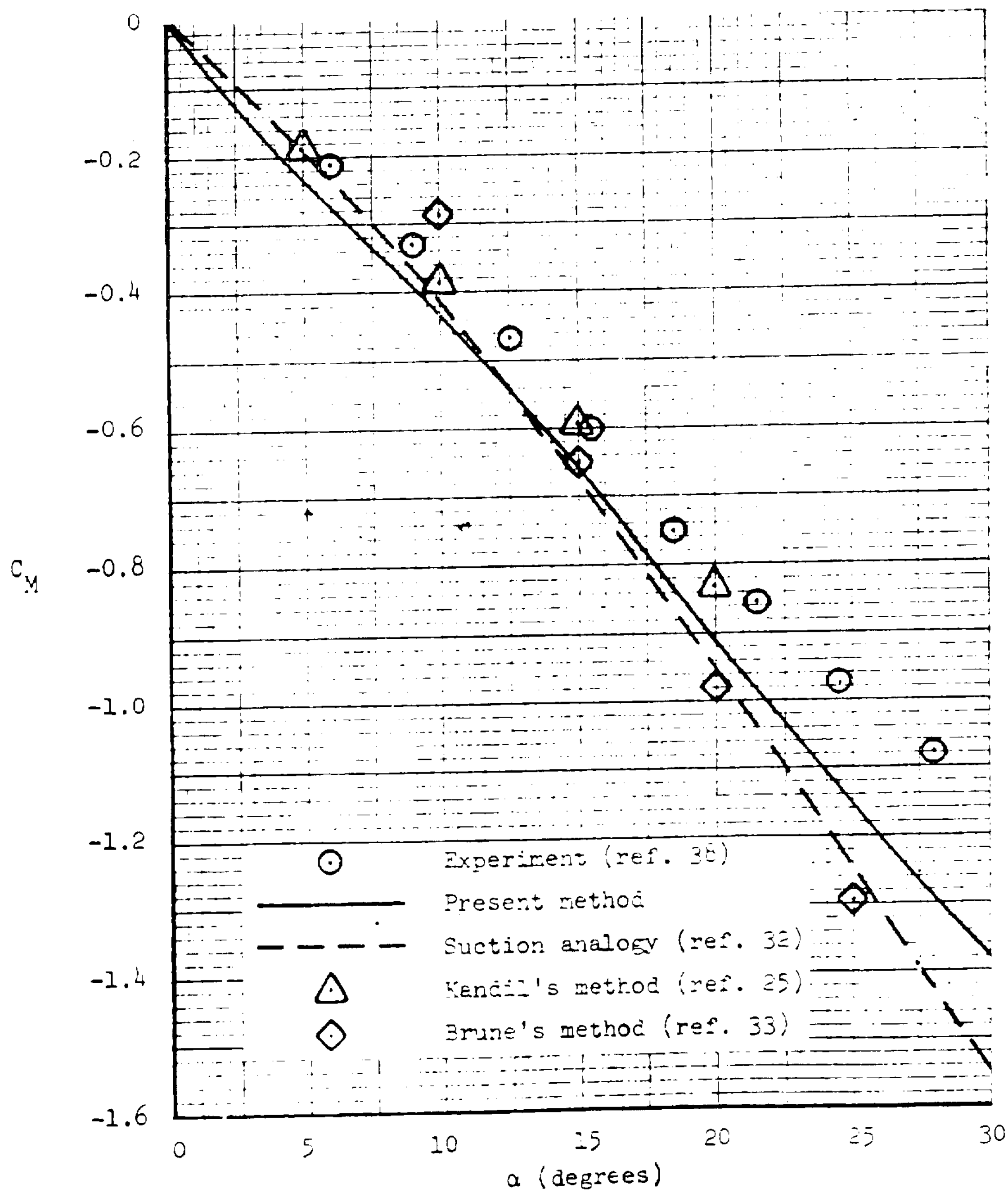

Figure 19b. Variation of pitching moment (about apex) coefficient with angle of attack for aspect ratio 2.0 delta wing

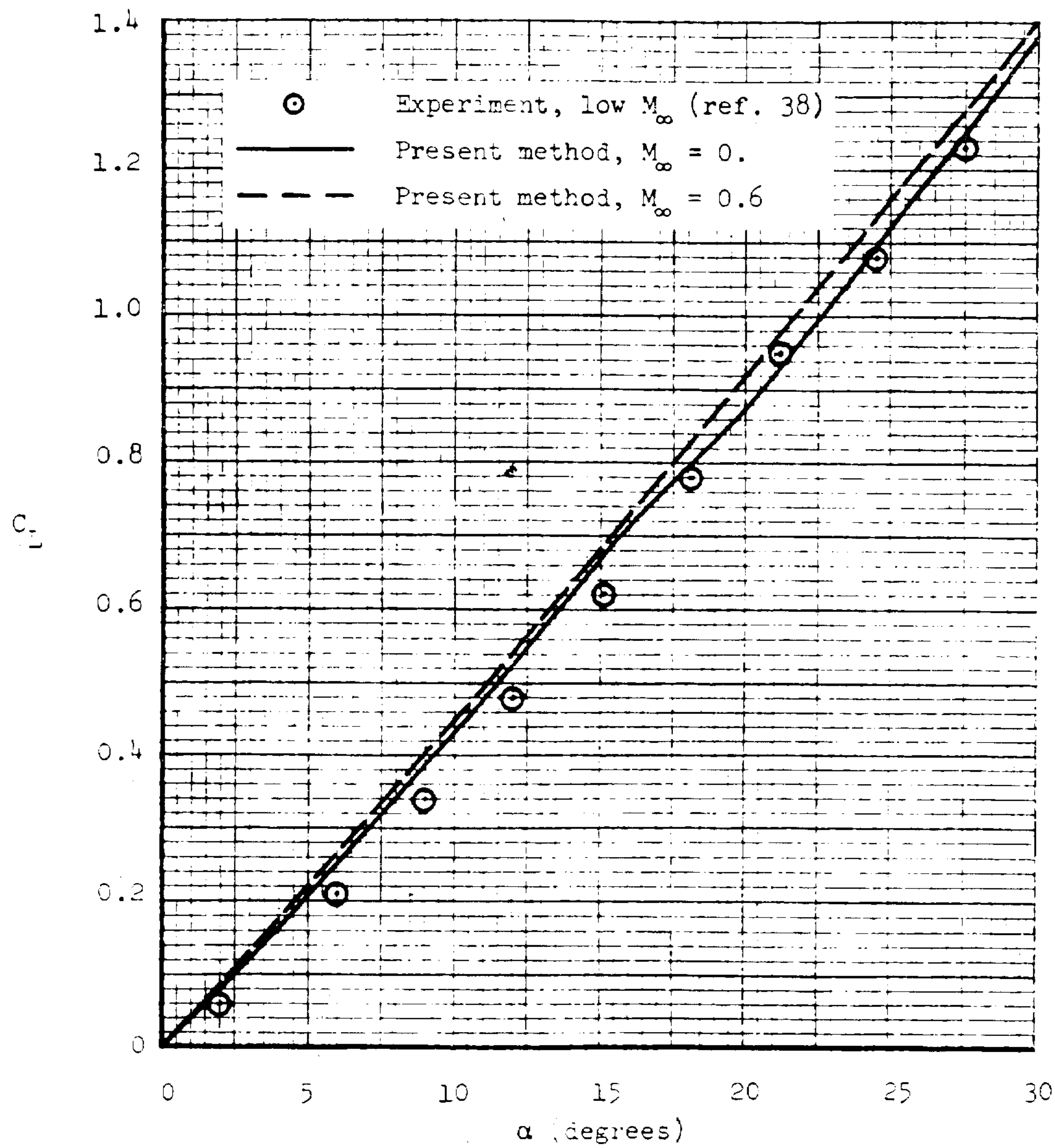

Figure 20a. Variation of lift coefficient with angle of attack for aspect ratio 1.5 delta wing at M_∞=0. and 0.6

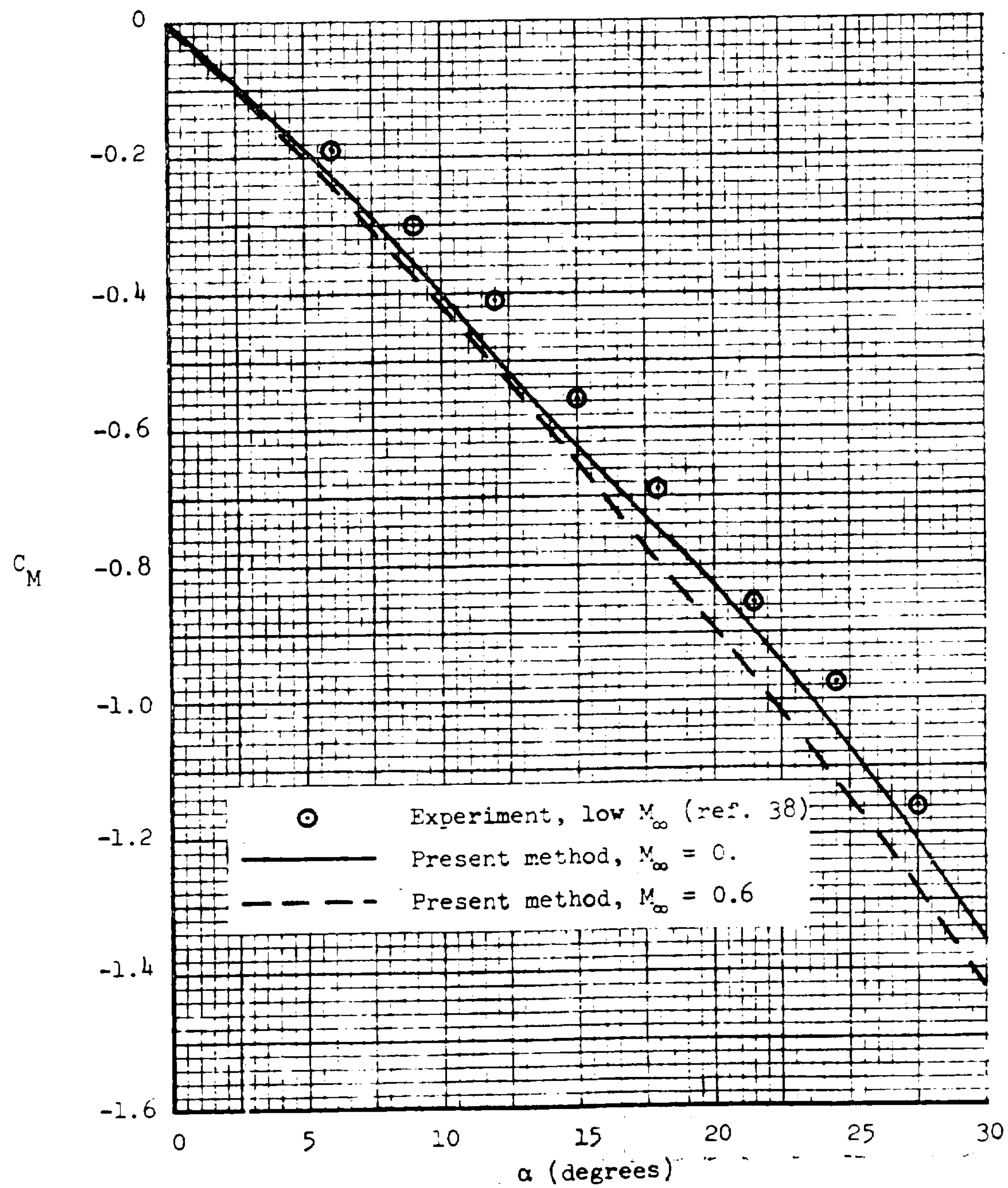

Figure 20b. Variation of pitching moment (about apex) coefficient with angle of attack for aspect ratio 1.5 delta wing at M_∞ = 0. and 0.6

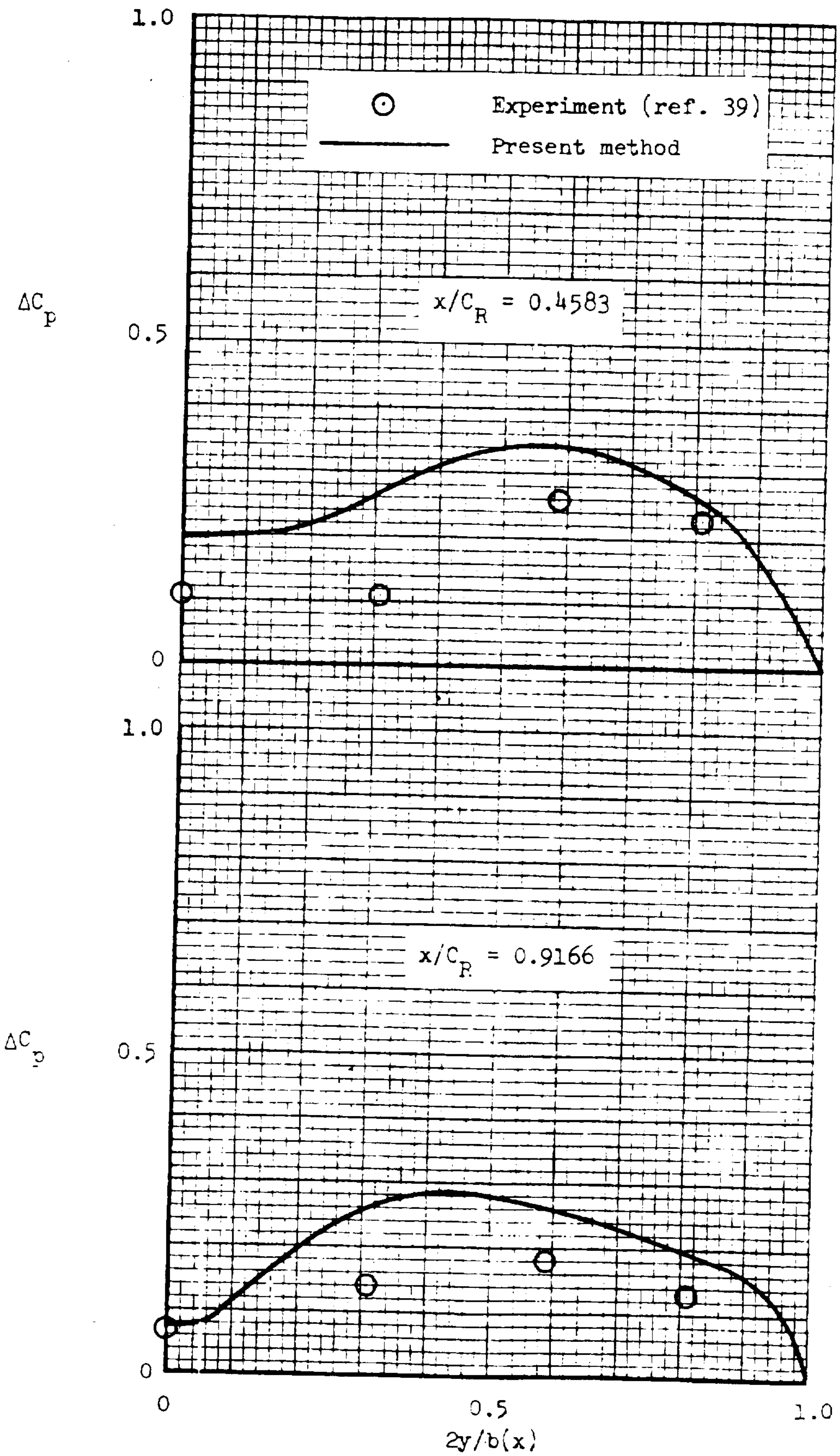

Figure 21. ΔC_p distribution for aspect ratio 0.7053 delta wing at 10.0 degree angle of attack

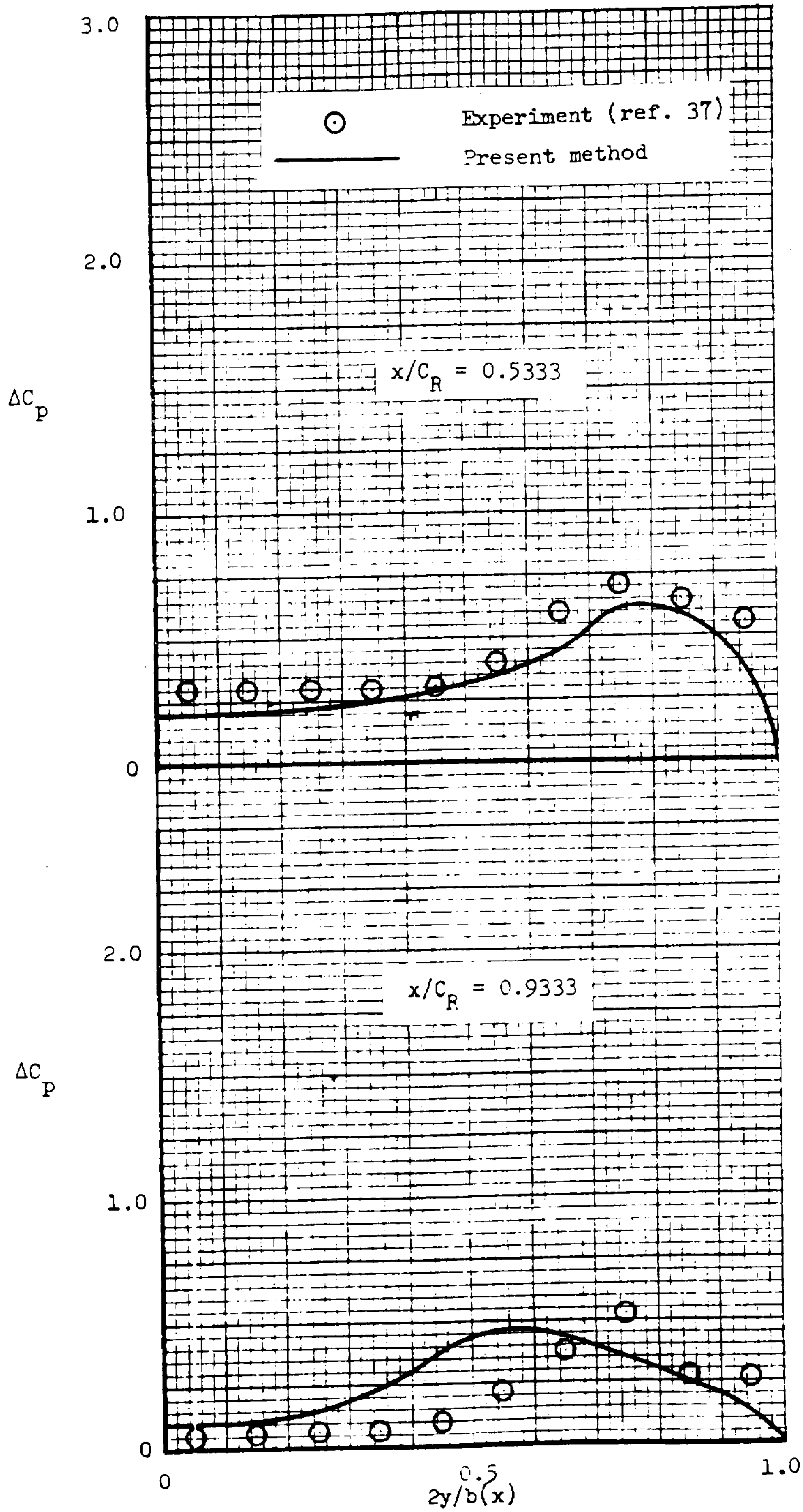

ORIGINAL PAGE IS OF POOR QUALITY

Figure 22a. ΔC_p distribution for aspect ratio 1.147 delta wing at 10.2 degree angle of attack

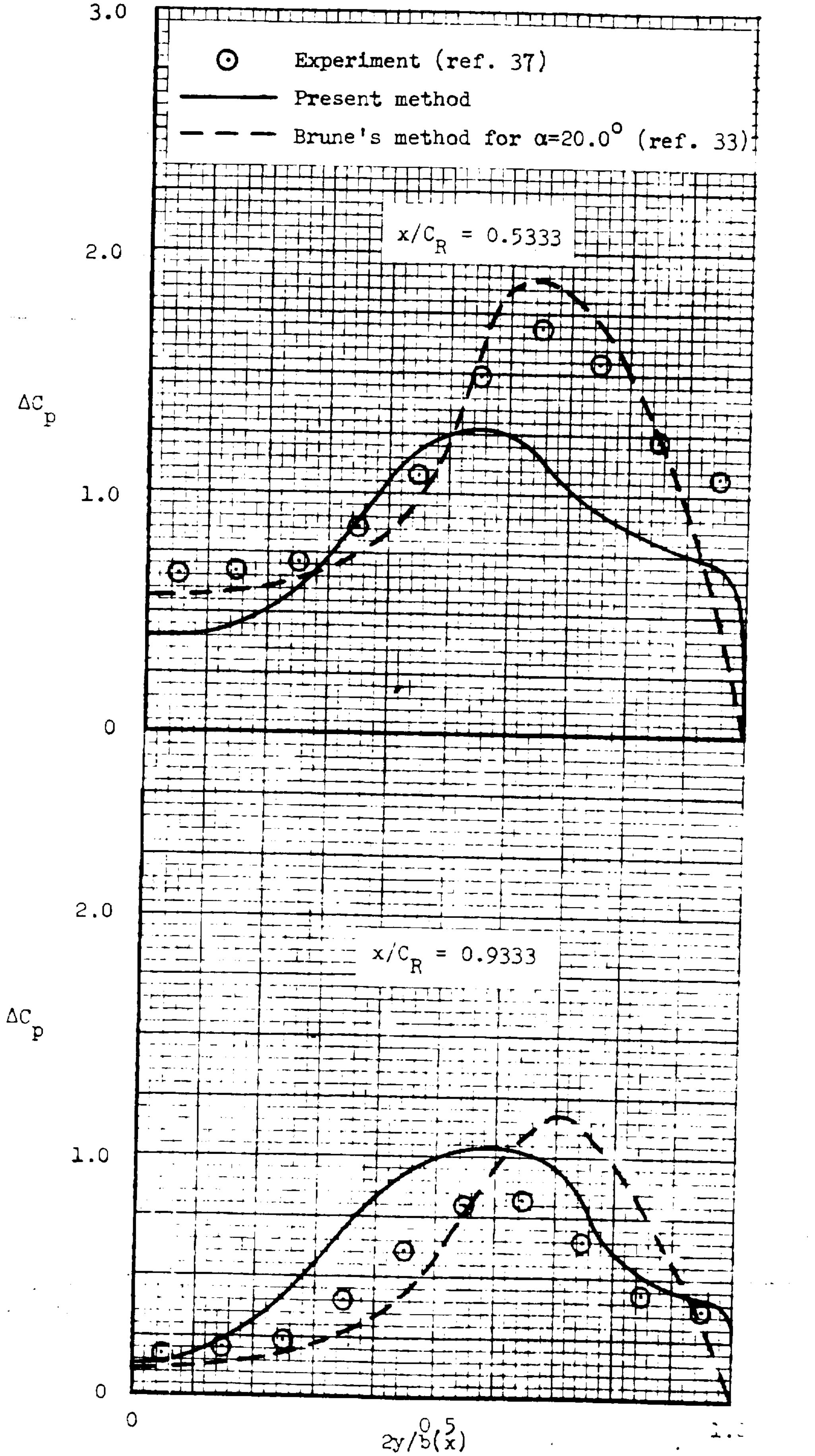

Figure 22b. ΔC_p distribution for aspect ratio 1.147 delta wing at 20.4 degree angle of attack

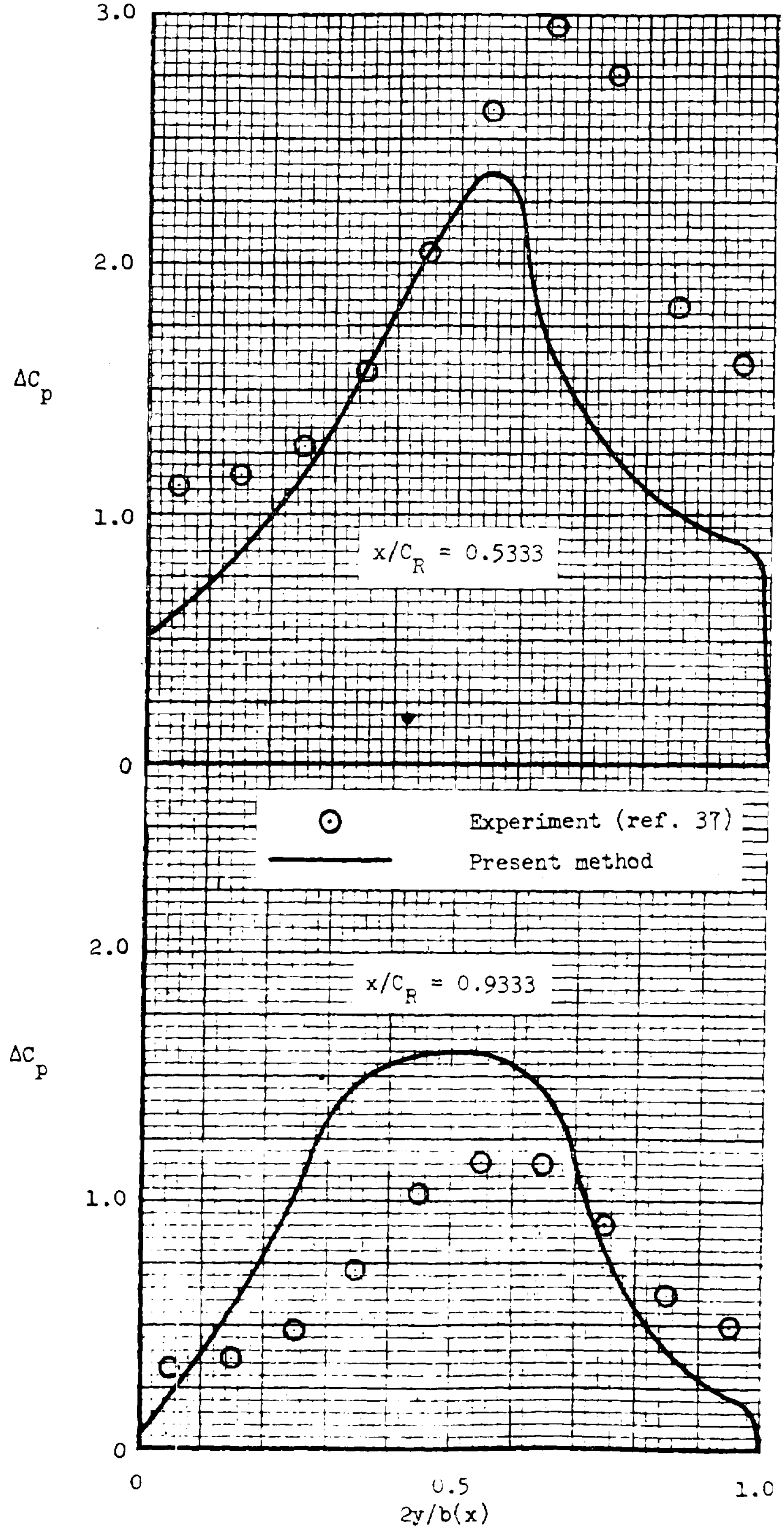

ORIGINAL PAGE IS
OF POOR QUALITY

Figure 22c. ΔC_p distribution for aspect ratio 1.147 delta wing at 30.7 degree angle of attack

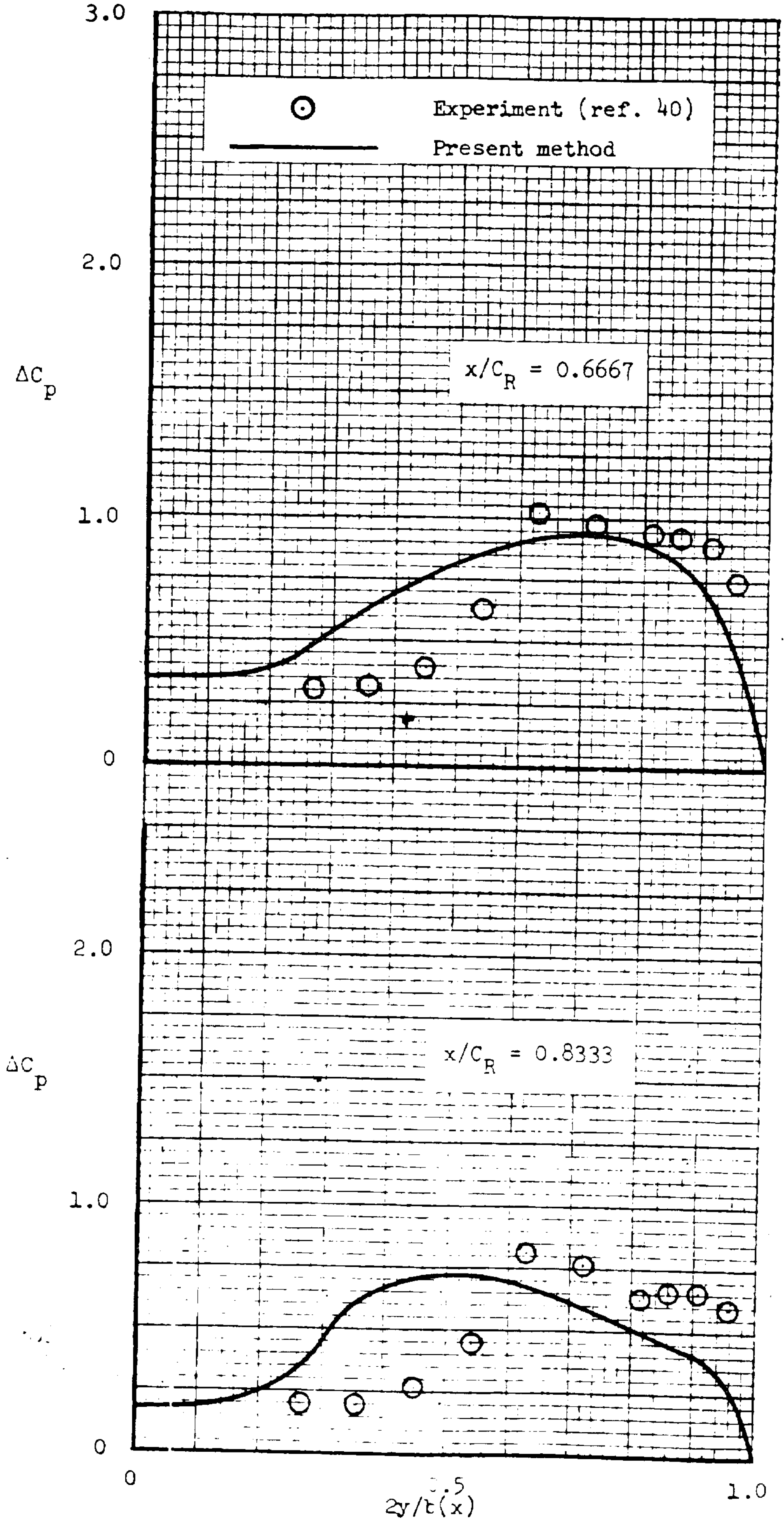

Figure 23a. ΔC_p distribution for aspect ratio 1.4559 delta wing at 14.0 degree angle of attack

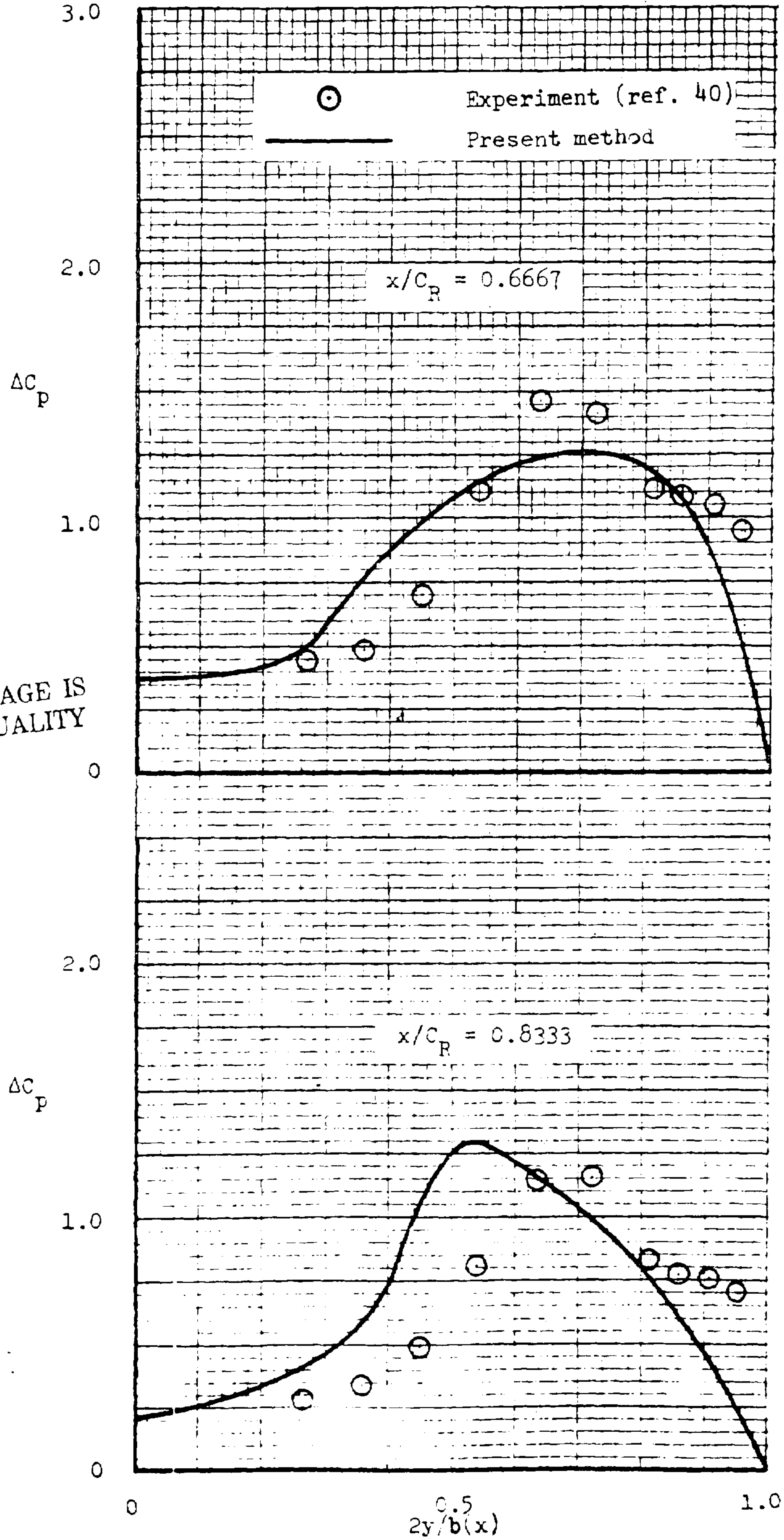

ORIGINAL PAGE IS
OF POOR QUALITY

Figure 23b. ΔC_p distribution for aspect ratio 1.4559 delta wing at 19.1 degree angle of attack

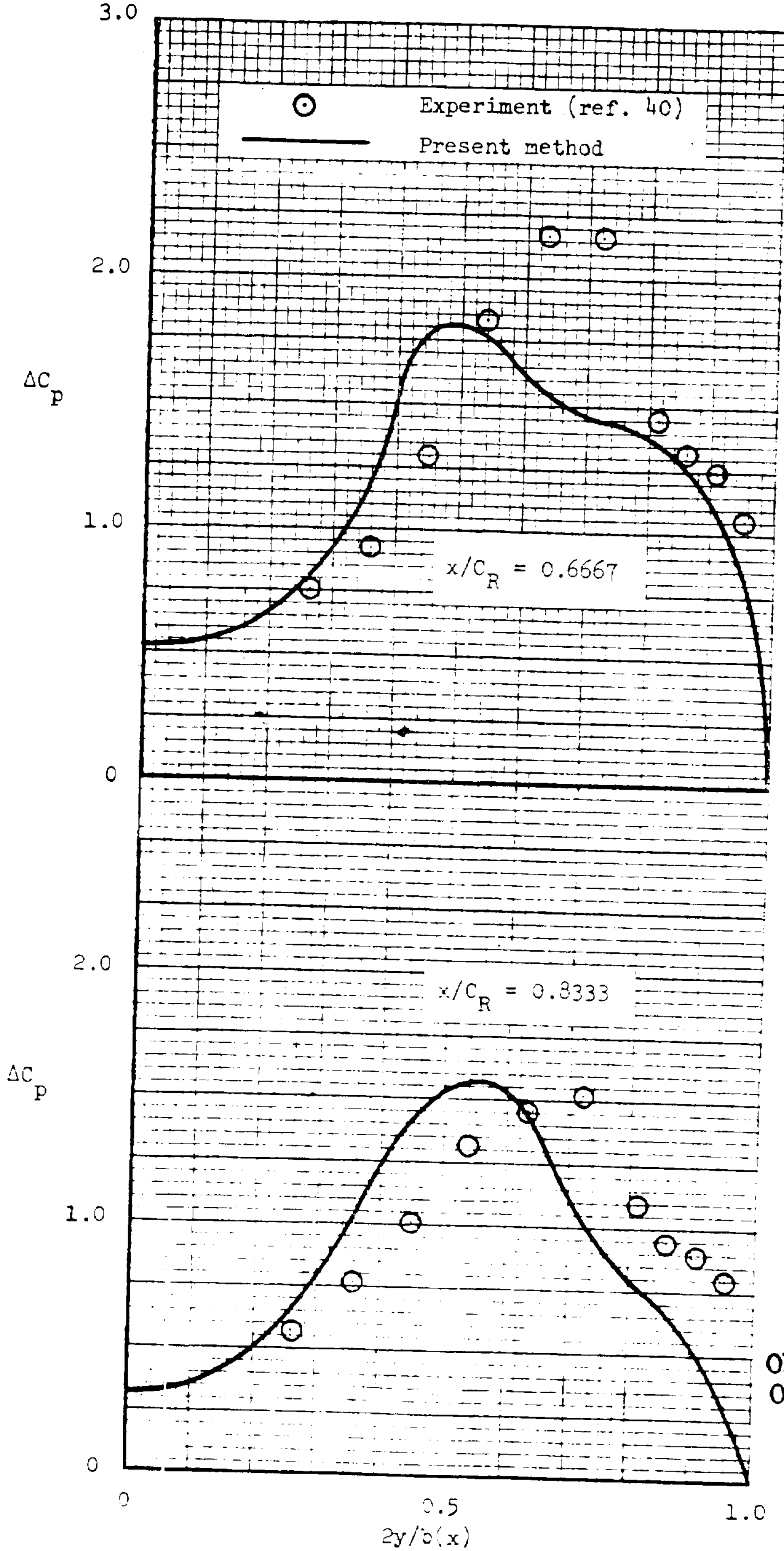

ORIGINAL PAGE IS OF POOR QUALITY

Figure 23c. ΔC_p distribution for aspect ratio 1.4559 delta wing at 23.9 degree angle of attack

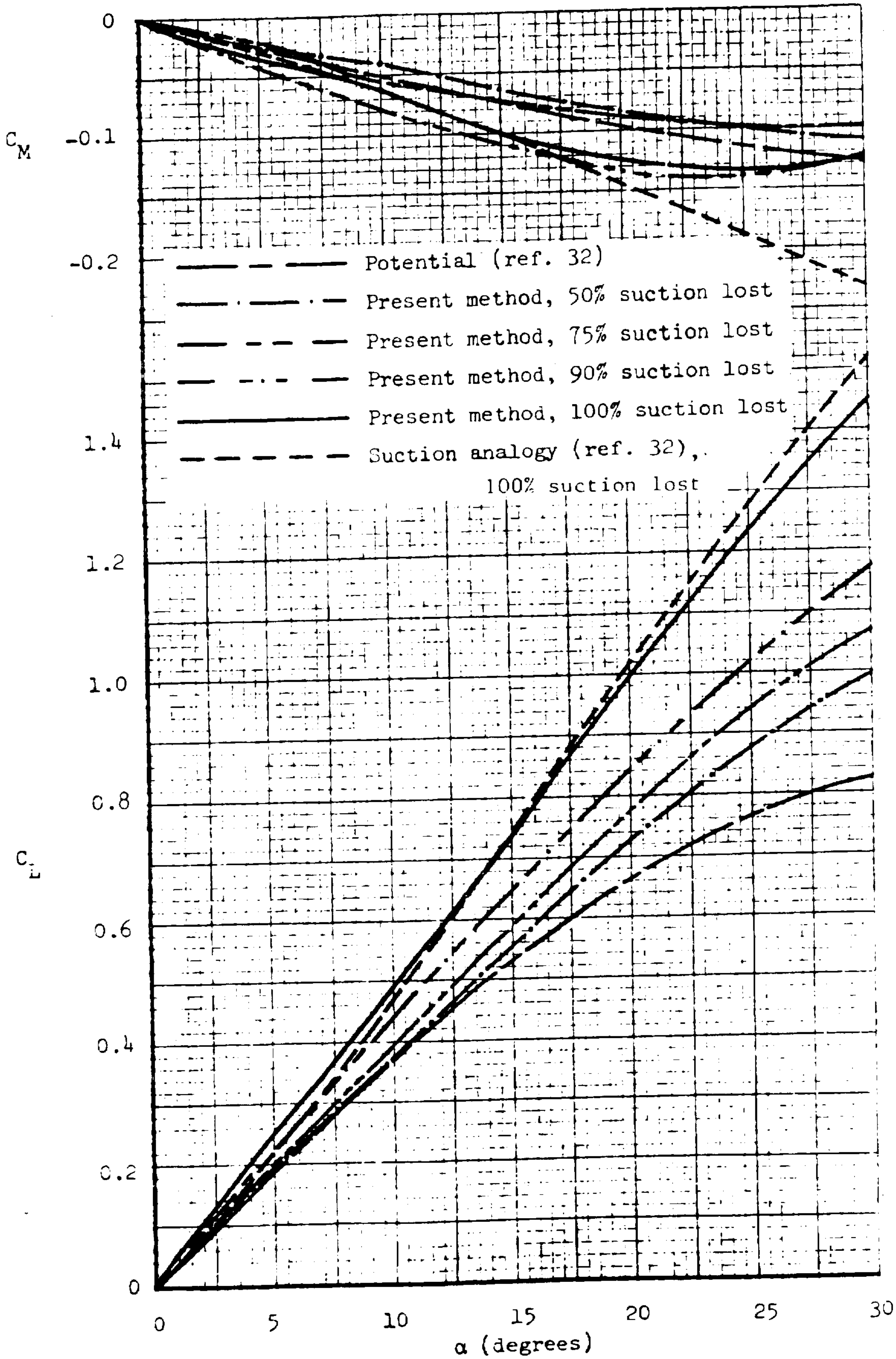

Figure 24a. Variation of lift and pitching moment (about 0.25$\bar{C}$) coefficient with angle of attack for aspect ratio 2.0 delta wing for different amounts of leading-edge suction

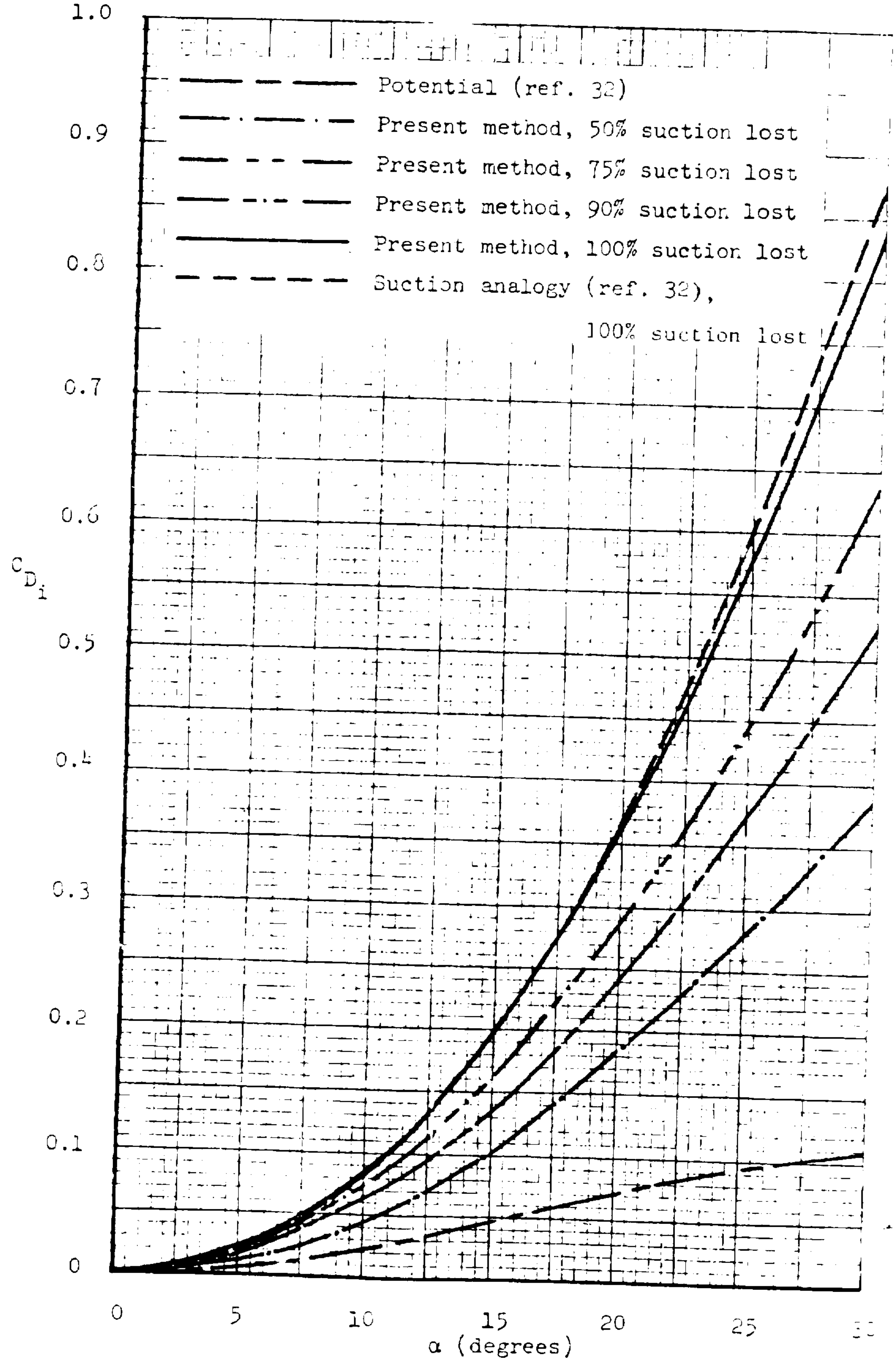

Figure 24b. Variation of induced drag coefficient with angle of attack for aspect ratio 2.0 delta wing for different amounts of leading-edge suction

1. Report No. NASA CR - 145304	2. Government Accession No.	3. Recipient's Catalog No.
4. Title and Subtitle A THEORETICAL INVESTIGATION OF THE AERODYNAMICS OF LOW-ASPECT-RATIO WINGS WITH PARTIAL LEADING-EDGE SEPARATION		5. Report Date January 1978
		6. Performing Organization Code
7. Author(s) Sudhir Chandra Mehrotra and C. Edward Lan		8. Performing Organization Report No. CRINC-FRL-266-1
9. Performing Organization Name and Address The University of Kansas Center for Research, Inc. 2291 Irving Hill Road - Campus West Lawrence, Kansas 66044		10. Work Unit No. 505-11-16-07
		11. Contract or Grant No. NSG-1046
		13. Type of Report and Period Covered Contractor Report
12. Sponsoring Agency Name and Address National Aeronautics and Space Administration Washington, DC 20546		14. Sponsoring Agency Code

15. Supplementary Notes

Langley technical monitor - Dr. John E. Lamar

16. Abstract

A numerical method is developed to predict distributed and total aerodynamic characteristics for low aspect-ratio wings with partial leading-edge separation. The flow is assumed to be steady and inviscid. The wing boundary condition is formulated by the Quasi-Vortex-Lattice method. The leading-edge separated vortices are represented by discrete free vortex elements which are aligned with the local velocity vector at mid-points to satisfy the force free condition. The wake behind the trailing-edge is also force free. The flow tangency boundary condition is satisfied on the wing, including the leading- and trailing-edges. Comparison of the predicted results with complete leading-edge separation has shown reasonably good agreement. For cases with partial leading-edge separation, the lift is found to be highly nonlinear with angle of attack.

17. Key Words (Suggested by Author(s))	18. Distribution Statement
Leading-Edge Separation Vortex Elements Leading-Edge Thrust Low Aspect-Ratio Wings High Angle-of-Attack	Unclassified - Limited Star Category - 02

19. Security Classif. (of this report)	20. Security Classif. (of this page)	21. No. of Pages	22. Price*
Unclassified	Unclassified	83	$6.00

* For sale by the National Technical Information Service, Springfield, Virginia 22161